Bam complex associated proteins in *Escherichia coli* are functionally linked to peptidoglycan biosynthesis, membrane fluidity and DNA replication

Jack A. Bryant[1,2*†], Kara A. Staunton[1†], Hannah M. Doherty[1], Micheal B. Alao[1], Xuyu Ma[1], Joanna Morcinek-Orłowska[3], Emily C. A. Goodall[4], Jessica Gray[4], Mathew Milner[1,5,6], Jeffrey A. Cole[1], Felicity de Cogan[7], Timothy J. Knowles[1], Monika Glinkowska[3], Danesh Moradigaravand[5,6*], Ian R. Henderson[4*], Manuel Banzhaf[1,8*].

† These authors contributed equally.

* Correspondence should be addressed to Jack A. Bryant – jack.bryant@nottingham.ac.uk, Manuel Banzhaf – manuel.banzhaf@newcastle.ac.uk, Danesh Moradigaravand - danesh.moradigaravand@kaust.edu.sa, or Ian R. Henderson - i.henderson@imb.uq.edu.au

[1]Institute of Microbiology and Infection, School of Biosciences, University of Birmingham, Edgbaston, B15 2TT, United Kingdom,

[2]School of Life Sciences, University of Nottingham, Nottingham, NG7 2RD, United Kingdom,

[3]Department of Biology, University of Gdańsk, 80-308 Gdańsk, Poland,

[4]Institute for Molecular Bioscience, University of Queensland, St. Lucia, 4072, Australia.

[5]Laboratory for Infectious Disease Epidemiology, KAUST Smart-Health Initiative and Biological and Environmental Science and Engineering Division, King Abdullah University of Science and Technology, Thuwal, Makkah 23955-6900, Saudi Arabia

[6]KAUST Computational Bioscience Research Center, King Abdullah University of Science and Technology, Thuwal, Makkah 23955-6900, Saudi Arabia

[7]School of Pharmacy, University of Nottingham, Nottingham, NG7 2RD, United Kingdom,

[8]Newcastle University Biosciences Institute, Faculty of Medical Sciences, Newcastle University, Newcastle upon Tyne, NE2 4HH, UK.

Abstract

Biogenesis of the bacterial outer membrane is key to bacterial survival and antibiotic resistance. Central to this is the β-barrel assembly machine (Bam) complex and its associated chaperones, which are responsible for transport, folding and insertion of outer membrane proteins (OMPs). The *Escherichia coli* Bam complex is composed of two essential subunits, BamA and BamD, and three non-essential accessory lipoproteins, BamB, BamC and BamE. Optimal Bam function is further dependent on the non-essential periplasmic chaperones DegP, Skp and SurA. Despite intensive study, the specific function of these non-essential Bam-associated proteins remains unknown. Here, we analysed Δ*bamB*, Δ*bamC*, Δ*bamE*, Δ*surA*, Δ*skp* and Δ*degP* knockout strains by phenotypic screening, conservation analysis and high-throughput genetics. We reveal that Bam complex activity is impacted by changes in outer membrane lipid composition and that enterobacterial common antigen is essential in the absence of the chaperone SurA. We also show components of peptidoglycan are conditionally essential with Bam accessory lipoproteins and that DNA replication control is perturbed in the absence of specific OMP assembly components. Together, our data indicates potential mechanisms for coordination of OMP biogenesis with other cellular growth processes such as LPS and peptidoglycan biogenesis, and DNA replication control.

Keywords:

Bam complex / TraDIS / Escherichia coli / DNA replication / peptidoglycan synthesis

Introduction

The Gram-negative outer membrane is instrumental for virulence, antimicrobial resistance, and immune evasion. The outer membrane is an asymmetric lipid bilayer consisting of phospholipid on the inner leaflet, lipopolysaccharide (LPS) on the outer leaflet, integral outer membrane proteins (OMPs) and associated lipoproteins. Biogenesis of the outer membrane is completed by several multi-component proteinaceous machines. Central to this is the β-barrel assembly machine (Bam) complex, the essential protein machinery responsible for folding and insertion of OMPs into the outer membrane, which then act as transporters, porins, receptors, virulence factors, adhesins and enzymes [1, 2]. All OMPs are synthesised in the cytoplasm before being trafficked through the inner membrane to the periplasmic space by the Sec machinery. OMPs are prone to aggregation and must be maintained in an unfolded state during their translocation to the Bam complex [3]. Three quality control proteins that chaperone OMPs across the periplasm are SurA, Skp and DegP, the latter of which also serves as a protease to degrade misfolded OMPs in the periplasm. The double mutants Δ*surA*Δ*skp* and Δ*surA*Δ*degP* are not viable, which suggests that Skp, SurA and DegP might be functionally redundant [4]. The primary chaperone pathway to the Bam complex is thought to be SurA, while Skp and DegP are suggested to form a secondary pathway that is amplified in stress conditions [5]. However, single molecule studies with purified OmpC and Skp or SurA demonstrate that the two proteins recognise different conformations of the OMP and that while Skp is capable of dispersing aggregated OmpC, SurA is not [6]. In addition, the absence of SurA increases degradation of OMPs that have stalled on the Bam complex, whereas loss of Skp in this scenario has the opposite effect, enhancing their assembly [7]. This is potentially due to the role of Skp in recognising and removing stalled OMP substrates from the Bam complex before being degraded alongside the misfolded OMP by the protease DegP [8]. Together, these studies challenge the long-standing assumption that these pathways are redundant and suggests that Skp and SurA have specialised roles in maintaining OMPs in a folding competent state during periplasmic transit.

74 Following transport across the periplasmic space, OMPs are received at the outer membrane
75 by the Bam complex. In *Escherichia coli*, the Bam complex is composed of two essential
76 subunits, the outer membrane β-barrel BamA and the lipoprotein BamD, and three non-
77 essential accessory lipoproteins, BamB, BamC and BamE [9, 10]. BamA is the central
78 component of the complex and consists of a 16-stranded β-barrel and five periplasmically
79 localised POlypeptide-TRansport-Associated (POTRA) domains that function to dock the
80 accessory subunits [11, 12]. The POTRA domains are hypothesised to interact with incoming
81 unfolded OMP substrates and feed them into the assembly machinery [13]. BamD is a
82 lipoprotein composed of five tetratricopeptide repeat (TPR) domains that interact with POTRA
83 5 of BamA [9, 14, 15]. The remaining components of the complex are the accessory
84 lipoproteins, BamB, BamC and BamE, which interact with BamA and BamD to form a
85 functionally coordinated ring structure under the BamA barrel on the periplasmic face of the
86 outer membrane [16-20].
87 The Bam complex accessory lipoproteins each contribute to full activity of the complex through
88 a shared redundant function of coordinating efficient BamA/D interaction in OMP engagement
89 and folding. Beyond this shared function, there is some limited information about specific roles
90 of these proteins in the cell [10, 21]. For example, as part of the Rcs stress response signalling
91 pathway, the outer membrane lipoprotein RcsF is threaded through an OMP during folding by
92 the Bam complex. This process specifically requires BamE to directly interact with and
93 coordinate BamA and BamD to enable completion of OMP folding around RcsF [22-24]. Lethal
94 jamming of the Bam complex in the absence of BamE can be prevented by BamB [23, 25].
95 BamB has also been shown to be important in folding of high-flux substrates [26]. However,
96 further information about the specific roles of BamB, BamC and BamE are lacking [21].
97 In this study, we provide evidence for specialised functions and show that changes to LPS
98 structure lead to increased membrane fluidity and decreased Bam complex activity. We also
99 identify that the cyclic form of enterobacterial common antigen (ECA), a periplasmic
100 carbohydrate, is essential in the absence of the chaperone protein SurA. We demonstrate that

101 the Bam accessory lipoproteins, including BamC, are essential in the absence of the
102 peptidoglycan stem-peptide component *meso*-DAP, providing a strong phenotype for this
103 poorly understood protein. Lastly, we show that loss of BamB causes the cells to over-initiate
104 DNA replication, indicating potential coordination between OMP biogenesis and DNA
105 replication. Together, our data indicate specialised roles for the Bam-associated proteins and
106 highlights potential mechanisms for coordination of OMP biogenesis with processes such as
107 outer membrane lipid biogenesis, peptidoglycan synthesis and DNA replication control.
108

109 **Results**

110 **Loss of Bam-associated proteins leads to distinct phenotypes**

111 We hypothesised that if the Bam-associated proteins have specialised roles in the cell it would
112 be unlikely that they phenocopy each other. Therefore, we tested fitness of Δ*bamB*, Δ*bamC*,
113 Δ*bamE*, Δ*surA*, Δ*skp* and Δ*degP* mutants of *E. coli* K-12 BW25113 compared to the parent
114 strain under various stresses. We arrayed the strains in 384-well format on solid agar plates
115 containing each stress or compound. Endpoint pictures were taken to quantify colony fitness
116 based on size by the image analysis software Iris [27]. Fitness was scored using the chemical
117 genomics analysis software ChemGAPP Small by comparing the mean colony size for the
118 mutant in each condition to the mean colony size of that mutant in the LB agar condition, which
119 was normalised to a fitness score of 1 [28]. Fitness scores below 1 represent decreased
120 fitness, as a function of colony size compared to growth on LB agar, and scores above 1
121 indicate increased fitness in that condition.

122 The fitness of each mutant across all conditions identified that the Δ*bamB* and Δ*surA* mutants
123 have the strongest fitness defects **(Fig 1)**. Correlation between each mutant fitness profile pair
124 was assessed by calculating the Pearson correlation coefficient. This demonstrated that
125 Δ*bamB* and Δ*surA* have a similar phenotypic profile with a correlation coefficient of 0.74, the
126 highest of all pairs of mutants **(Fig S1)**. Similar decreased fitness scores were observed for
127 both strains in the presence of bacitracin, carbenicillin, erythromycin, sodium dodecyl-sulfate

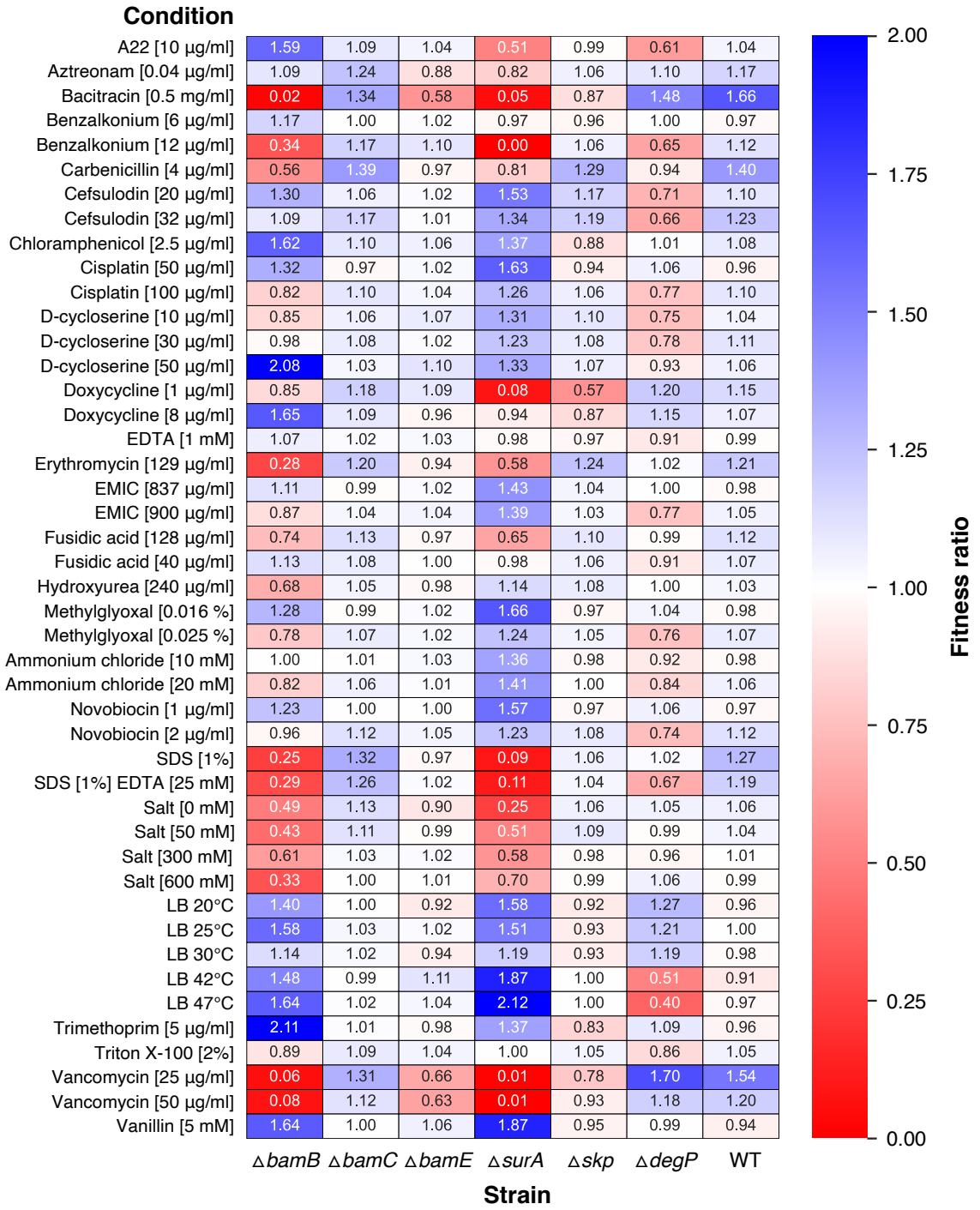

Figure 1 – Phenotypic profiling of mutants lacking Bam-associated proteins
Heat map of fitness scores for the *E. coli* BW25113 parent strain and Δ*bamB*, Δ*bamC*, Δ*bamE,* Δ*surA*, Δ*skp*, or Δ*degP* mutants grown in various stress conditions. Colony size measurements for each condition were normalised by comparing to colony size of that strain when grown on LB medium at 37°C. Growth of each strain on LB is set to 1 and each condition normalised to this. Fitness scores above 1 represent better growth than the LB condition as measured by colony size and scores below 1 indicate smaller colony size than the LB condition. Some conditions are abbreviated due to space restrictions: EMIC - 1-Ethyl-3-methylimidazolium chloride, EDTA - Ethylenediaminetetraacetic acid, SDS – Sodium dodecyl sulfate.

140 (SDS), osmotic stress conditions due to varied salt concentrations, and vancomycin **(Fig 1)**.
141 This is unsurprising as SurA is the major chaperone pathway for OMPs to reach the Bam
142 complex resulting in low fitness of Δ*bamB* and Δ*surA* when growing on LB at 37°C. However,
143 they do not phenocopy in all conditions. For example, the Δ*bamB* strain grew better in the
144 presence of the MreB inhibitor A22 with a fitness score of 1.59, but the Δ*surA* mutant was less
145 fit in this condition (score of 0.51). They also had opposing fitness scores in the presence of
146 doxycycline (Δ*bamB* – 1.65, Δ*surA* – 0.94) and hydroxyurea (Δ*bamB* – 0.68, Δ*surA* – 1.14)
147 **(Fig 1)**. The Δ*bamE* mutant mildly correlated to Δ*bamB* with a coefficient of 0.51 **(Fig S1)**.
148 However, both mutants were sensitive to vancomycin (Δ*bamB* – 0.06, Δ*bamE* – 0.66) and
149 bacitracin (Δ*bamB* – 0.02, Δ*bamE* – 0.58) two antibiotics that exceed the exclusion limit of
150 outer membrane porins and to which sensitivity indicates damage to the permeability barrier.
151 In contrast, Δ*bamC* has no strong phenotypes and correlated most strongly with the WT parent
152 strain **(Fig 1 and Fig S1**). Similarly to Δ*bamC*, the Δ*skp* mutant also has no strong phenotypes
153 in our screen. The Δ*degP* strain was negatively correlated with the other periplasmic
154 chaperone pathway group mutants Δ*skp* (-0.51) and Δ*surA* (-0.37) and with Δ*bamE* (-0.68)
155 due to opposing fitness scores in a range of stresses **(Fig. 1 and Fig S1)**. Interpretation of this
156 result is complicated by DegP not only functioning as a chaperone, but also as a protease that
157 targets misfolded OMPs in the periplasm [29]. However, due to the role of DegP in degrading
158 stalled OMPs that have been recognised by Skp, they might have been expected to correlate
159 [8]. Together, the phenotypic profiling data indicate that while there are shared phenotypes
160 between each knockout, we observe a broad range of unique, mutant specific phenotypes that
161 suggests specialised roles beyond those observed previously.
162
163 **TraDIS identifies unique synthetic lethal interactions for Bam-associated proteins.**
164 Considering that the Bam-associated proteins have specialised function, we sought to find
165 their genetic interaction networks by using Transposon-Directed Insertion site Sequencing
166 (TraDIS). When TraDIS libraries are generated in single gene deletion mutant backgrounds,

167 the insertion frequencies of genes/regions compared to wild-type cells identifies genes that
168 become more important for survival in the mutant backgrounds. These genes are termed
169 conditionally essential, and help to identify co-dependencies of processes that the candidate
170 gene might be involved in. The method can also identify mutants that are more fit in the given
171 genetic background or condition [30-33]. Therefore, the parent strain (*E. coli* BW25113) and
172 Δ*bamB,* Δ*bamC,* Δ*bamE,* Δ*surA,* Δ*skp,* or Δ*degP* mutants were transformed with a mini Tn5-
173 kanamycin transposon and recovered on LB agar at 37°C. Transposon mutants were then
174 pooled and transposon insertion sites identified by DNA sequencing as described previously
175 [32]. The BioTraDIS pipeline was used for data analysis to classify genes as either essential
176 or non-essential. Essential genes were then compared to the parent BW25113 TraDIS library
177 to identify genes that became essential in the knockout strains (conditionally essential) **(Table**
178 **S1)** [34]. For quality control, two independent replicates of each transposon library were
179 sequenced over several sequencing runs. Individual sequencing runs had a high correlation
180 coefficient of ≥0.93 between samples and generated >6 million TraDIS reads and >500,000
181 unique insertion sites for each strain **(Fig S2 and S3)**. Transposon insertion sites were evenly
182 mapped throughout the genome, with the exception of an increased density around the origin
183 of replication as expected due to gene dosage **(Fig S4)** [35].
184 These experiments are designed to identify novel genetic interactions, but this unbiased
185 approach will also uncover known synthetic lethal gene pairs that allow benchmarking of our
186 data. We confirmed known genetic interactions between *surA* and *skp* [4], *degP* and *surA* [4],
187 *bamB* and *degP* [26] and *bamE* and *bamB* [25, 36] **(Fig S5)**. The Δ*bamB,* Δ*bamC* and Δ*bamE*
188 TraDIS libraries allowed identification of 93, 92 and 29 conditionally essential genes,
189 respectively **(Fig 2A and Table S1)**. This is particularly surprising as there are no known roles
190 or dependencies for *bamC* and we did not observe strong phenotypes for Δ*bamC* in our
191 phenotypic screen **(Fig 1)**. Unfortunately, 54 of the genes identified as conditionally essential
192 in the Δ*bamC* background are of unknown function, therefore providing no hypotheses for the
193 role of BamC **(Table S1)**. We then compared the conditionally essential gene lists to probe if

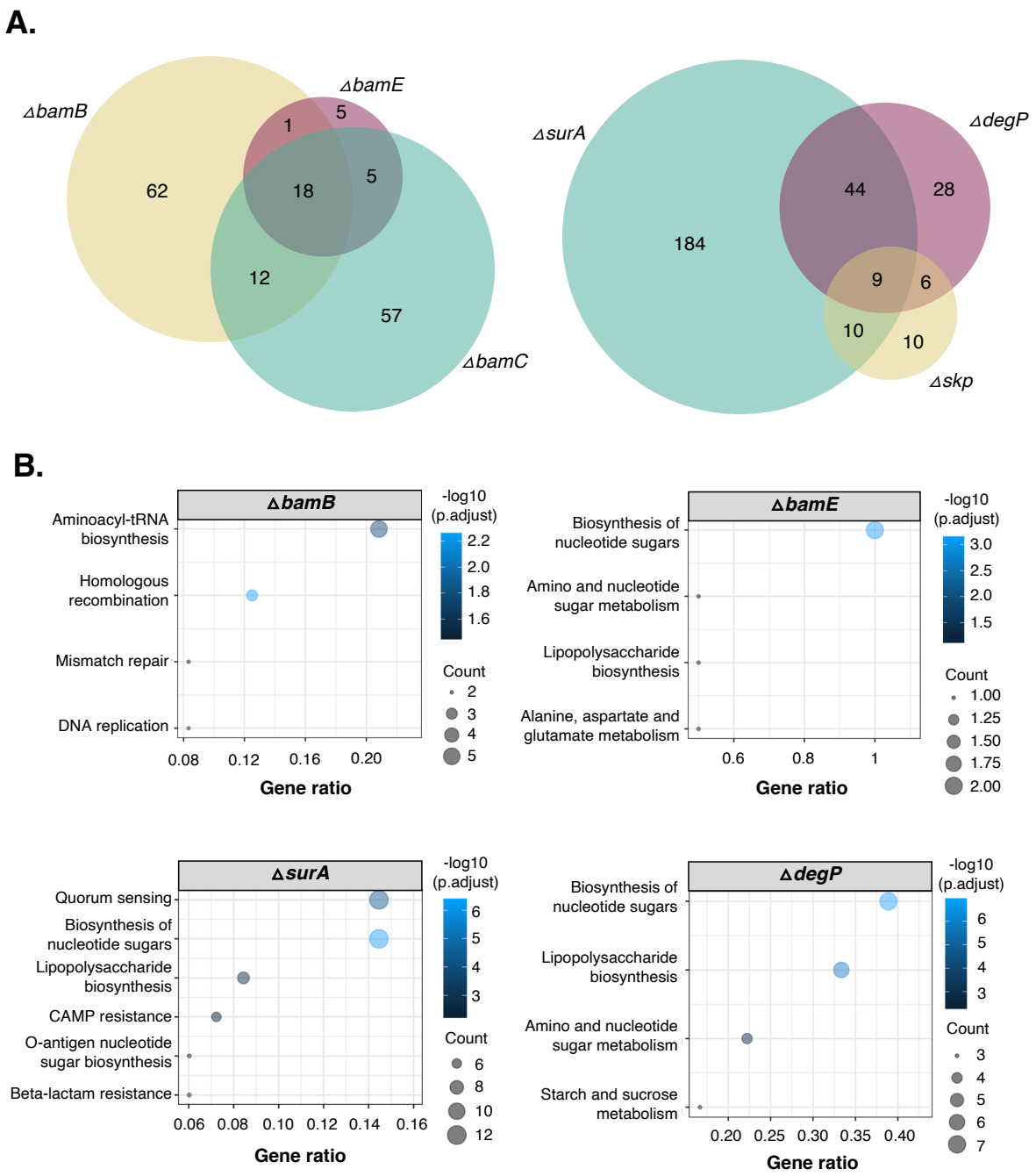

Figure 2 - Genetic interaction analysis of Bam-associated genes by TraDIS
TraDIS libraries were constructed in the *E. coli* BW25113 parent strain and Δ*bamB*, Δ*bamC*, Δ*bamE,* Δ*surA*, Δ*skp*, or Δ*degP* mutants to identify genes that become essential in each knockout strain compared to the parent library (conditionally essential). **A.** Venn diagrams showing conditionally essential genes identified within the Δ*bamB*, Δ*bamC* and Δ*bamE* TraDIS libraries or the Δ*surA*, Δ*skp* and Δ*degP* libraries. **B.** Analysis of KEGG categories enriched in conditionally essential gene lists in the Δ*bamB*, Δ*bamE,* Δ*surA* and Δ*degP* TraDIS libraries, represented as bubble plots. No data is shown for the Δ*bamC* and Δ*skp* conditionally essential gene lists as there was no significant enrichment of any KEGG categories.

206 they are involved in similar processes or contribute to the same function within the cell. In the
207 case that all three Bam accessory proteins solely contribute to Bam function, we would expect
208 to find significant overlap between mutants. However, we found many unique conditionally
209 essential genes for each (62, 57 and 5 for Δ*bamB,* Δ*bamC* and Δ*bamE,* respectively),
210 supporting the hypothesis that each has specialised roles in the cell **(Fig 2A)**.
211 For the OMP chaperone pathway mutants we identified 247, 87 and 35 conditionally essential
212 genes for the Δ*surA,* Δ*degP* and Δ*skp* mutants, respectively **(Fig 2A)**. The Δ*surA* mutant had
213 many strong phenotypes when probed against stresses **(Fig 1)**, which could explain the large
214 number of conditionally essential genes compared to the other OMP chaperone mutants **(Fig**
215 **2A)**. Of the 87 conditionally essential genes in the Δ*degP* dataset, only 15 were also in the
216 Δ*skp* background, despite DegP and Skp functioning together to degrade stalled OMP
217 substrates [8]. This difference is also potentially due to the dual role of DegP as both a
218 chaperone and a protease [29]. These results suggest that while there is functional
219 redundancy between the SurA and DegP/Skp chaperone pathways, the function of the
220 chaperones under specific chemical and genetic conditions is likely specialised **(Fig 1 and**
221 **2A)**.To determine the functions and associated pathways of the conditionally essential genes
222 identified in the mutant backgrounds, we completed GO and KEGG analyses. Enrichment
223 analysis of KEGG pathways for the Δ*bamC* and Δ*skp* datasets resulted in no significant
224 enrichment of any one category. However, genes involved in "Lipopolysaccharide
225 biosynthesis" and "Biosynthesis of nucleotide sugars" were enriched in the Δ*surA*, Δ*degP* and
226 Δ*bamE* conditionally essential gene lists and "O-antigen nucleotide sugar biosynthesis" was
227 enriched in the Δ*surA* background **(Fig 2B and Table S2)**. The most enriched KEGG pathway
228 in the Δ*bamB* dataset was "Aminoacyl-tRNA biosynthesis", however these genes all encode
229 tRNAs and are on average 75 bp in length. Visual inspection of these gene regions identified
230 sparse insertion density within the local genomic area leading to a likely false positive for
231 conditional essentiality. The Δ*bamB* dataset is also significantly enriched for three other KEGG
232 pathways: "Homologous recombination", "Mismatch repair" and "DNA replication" **(Fig 2B and**
233 **Table S2)**. Together, the KEGG pathway enrichment analysis identifies the importance of LPS

234 and ECA biosynthesis in these mutants as well as a potential link between OMP biogenesis
235 and DNA replication. This directed our further investigations.
236
237 **Genes required for heptose incorporation into LPS are synthetically lethal with *bamB,***
238 ***surA* and *degP***
239 We identified that fewer mutants were recovered with transposon insertions in genes involved
240 in LPS assembly in the Δ*bamB*, Δ*surA* and Δ*degP* backgrounds than in the parent. In addition,
241 genes involved in "Biosynthesis of nucleotide sugars" were significantly enriched, with genes
242 identified being involved in the synthesis of heptose, a core component of LPS **(Fig 2B and**
243 **Table S2)**. Despite this category being enriched in the Δ*bamE* dataset, we found this was due
244 to one gene in particular, *glmS*, and that the result was actually specific to the Δ*bamB*, Δ*surA*
245 and Δ*degP* TraDIS libraries **(Fig 3A and Fig S6)**. Synthesis of heptose consists of five main
246 steps before it is incorporated into the LPS inner core **(Fig 3B)**. In the Δ*surA* and Δ*degP* TraDIS
247 libraries, all four genes involved in synthesis of heptose were essential: *gmhA*, *gmhB*, *hldE*
248 and *waaD*. In the Δ*bamB* background all were essential except for *gmhB,* which is potentially
249 because a Δ*gmhB* mutant is not completely devoid of heptose [37]. These data suggest that
250 heptose production was functionally more important in Δ*degP* and Δ*surA* than in the Δ*bamB*
251 mutant. The incorporation of heptose into the LPS structure was also functionally important.
252 In Δ*degP* and Δ*surA* mutants, the genes *waaC* and *waaF* were conditionally essential, which
253 are responsible for transfer of the first and second heptose onto the LPS inner core,
254 respectively **(Fig 3A and 3B)** [38, 39]. In contrast, in the Δ*bamB* mutant, *waaC* was
255 conditionally essential whereas *waaF* was not. This implies that while Δ*degP* and Δ*surA*
256 mutants are not able to tolerate having LPS with only one heptose residue, the Δ*bamB* mutant
257 is.
258
259 **LPS truncation increases membrane fluidity and decreases Bam complex activity**
260 Increased outer membrane fluidity decreases Bam activity and modifications to LPS structure
261 can lead to changes in membrane fluidity [40]. Thus, we hypothesised that changes in LPS

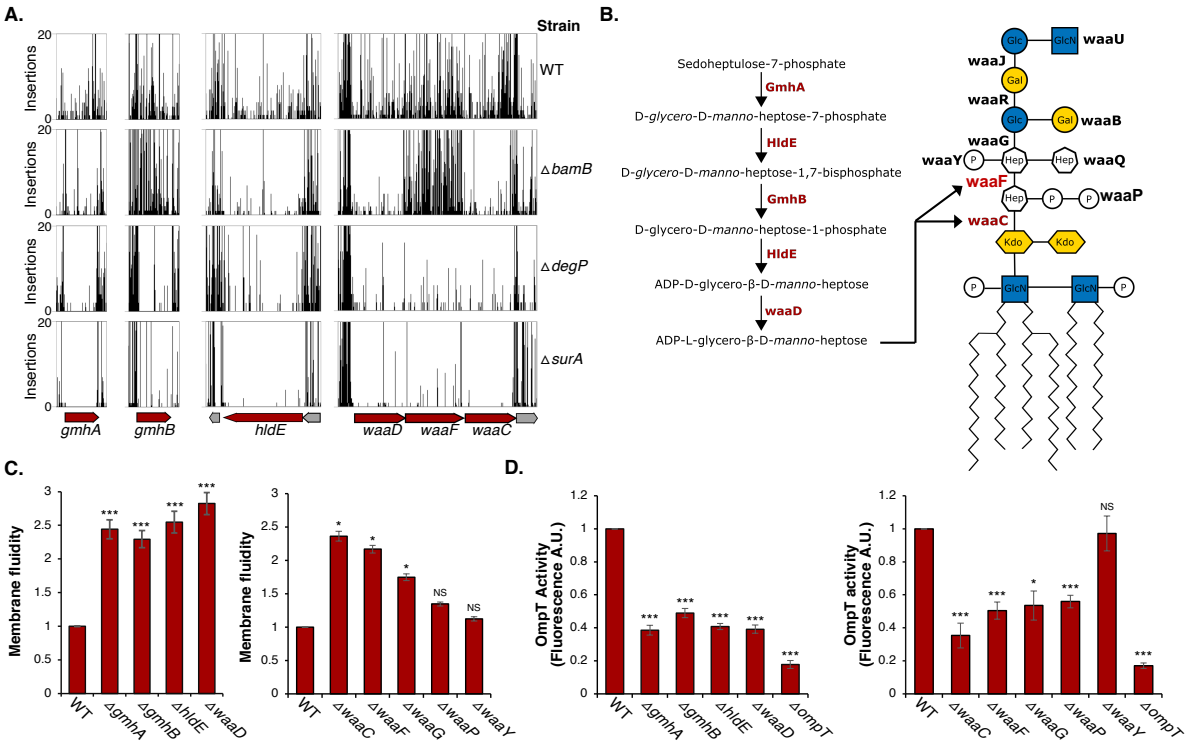

Figure 3 - Incorporation of heptose into LPS is essential in Δ*bamB*, Δ*surA* and Δ*degP*

A. Transposon insertions in the genes *gmhA*, *gmhB*, *hldE, waaD, waaC,* and *waaF* in the parent, Δ*bamB,* Δ*surA* and Δ*degP* TraDIS libraries. Transposon cut-off is set to 20. Essential genes are represented as red arrows. **B**. Schematic of the heptose biosynthesis pathway and LPS structure in *E. coli* K-12 BW25113 with gene labels for LPS biosynthesis enzymes indicated next to the linkage they form or component they ligate. Enzymes identified as conditionally-essential are labelled in red text. **C.** Membrane fluidity was measured in Δ*gmhA,* Δ*gmhB,* Δ*hldE,* Δ*waaD,* Δ*waaC*, Δ*waaF*, Δ*waaG*, Δ*waaP* and Δ*waaY* mutants and compared to the parent strain by using pyrenedeconoic acid fluorescence. **D.** To determine the extent of Bam complex activity, successful folding and insertion of OmpT into the outer membrane was measured in the Δ*gmhA,* Δ*gmhB,* Δ*hldE,* Δ*waaD,* Δ*waaC*, Δ*waaF*, Δ*waaG*, Δ*waaP*, Δ*waaY* and Δ*ompT* mutants and compared to the parent strain. For panels C and D, experiments were performed in biological and technical triplicate with standard deviation represented by error bars. Two sample t-tests were used to assess statistical significance of differences from the WT strain with *** indicating p-values of <0.001, * indicating p-values of <0.05, and NS as not significant (p-value ≥0.05).

279 core structure would affect membrane fluidity to differing degrees, which could affect Bam
280 complex efficiency. To test this hypothesis we assessed membrane fluidity and Bam complex
281 activity in strains lacking the genes encoding the heptose biosynthesis pathway (Δ*gmhA*,
282 Δ*gmhB,* Δ*hldE*, and Δ*waaD*) and LPS core synthesis (Δ*waaC*, Δ*waaF*, Δ*waaP*, Δ*waaG* and
283 Δ*waaY*) **(Fig 3)**. There were no differences in transposon insertion index for the gene *waaY,*
284 which encodes the enzyme responsible for phosphorylation of the second heptose in the LPS
285 inner core. Therefore, Δ*waaY* should act as a control in this experiment [41]. In addition,
286 Δ*waaP* and Δ*waaG*, which are responsible for phosphate addition to the first heptose, and
287 incorporation of the first glucose, respectively [42], were included as a small decrease in the
288 insertion indexes for these genes were observed in the Δ*surA* and Δ*degP* TraDIS datasets
289 **(Fig S7).**
290 Fluidity of the membrane for each mutant was measured using the lipophilic pyrene probe,
291 pyrene decanoic acid. The pyrene monomer can undergo excimer formation and
292 demonstrates a shift in fluorescence, a process which is dependent on the ease of mobility
293 within the membrane [43, 44]. Formation of the excimer was measured and compared to that
294 of the parent strain **(Fig 3C)**. The largest increase in membrane fluidity occurred in knockouts
295 of genes required for heptose biosynthesis: Δ*gmhA*, Δ*gmhB,* Δ*hldE*, and Δ*waaD*. Of this
296 group, the Δ*gmhB* mutant had the smallest increase in membrane fluidity and this gene was
297 also not essential in the Δ*bamB* background **(Fig 3A and 3C)**. Of the genes required for LPS
298 core biosynthesis, membrane fluidity was higher in Δ*waaC*, Δ*waaF* and Δ*waaG* than in the
299 parent strain with the biggest change being in Δ*waaC* and the smallest in Δ*waaG*. However,
300 there was no significant increase in fluidity in the Δ*waaP* mutant. Membrane fluidity of the
301 Δ*waaF*, Δ*waaP* and Δ*waaG* mutants was intermediate between that of the heptoseless
302 Δ*waaC* mutant and the parent, with the severity of the effect correlating to the severity of LPS
303 core truncation. No significant change in membrane fluidity was measured in the Δ*waaY*
304 mutant control **(Fig 3C)**.
305 Next, we investigated whether impairment of heptose synthesis affected activity of the Bam
306 complex, which was monitored by an *in vivo* OmpT fluorescence assay. The outer membrane

307 protease OmpT requires the Bam complex for folding and insertion into the membrane and is
308 able to cleave a fluorogenic peptide, which is monitored by increased fluorescence over time
309 [10]. Except for Δ*waaY*, all mutants demonstrated a minimum 40% decrease in OmpT activity
310 compared to the parent strain. The heptoseless Δ*waaC* mutant exhibited the greatest
311 decrease in OmpT activity. The effect of Δ*waaF*, Δ*waaP* and Δ*waaG* mutations on OmpT
312 activity levels was comparable to each other and intermediate between that of Δ*waaC* and the
313 parent strain **(Fig 3D)**. In summary, mutations that lead to heptoseless LPS had the biggest
314 increase in membrane fluidity and the lowest levels of OmpT activity with a graded response
315 based on the severity of LPS core truncations. This suggests there is a correlation between
316 LPS core structure, membrane fluidity and Bam complex activity that leads to a variety of Bam
317 complex activity levels depending on the form of LPS in the outer membrane.
318
319 **Generation of cyclic ECA is essential in the absence of the chaperone SurA**
320 Genes involved in 'Biosynthesis of nucleotide sugars' were significantly enriched as
321 conditionally essential in the Δ*surA* mutant. The genes identified are involved in biosynthesis
322 of ECA (**Fig 2B)**, which is a highly conserved carbohydrate-derived molecule present on the
323 external leaflet of the outer membrane and in the periplasm of Enterobacteriaceae [45, 46].
324 The ECA biosynthesis pathway genes were all conditionally essential with the exception of
325 *wxyE,* which is required for survival of both the parent and the Δ*surA* mutant **(Fig 4A and 4B)**.
326 In addition, fewer mutants were recovered with transposon insertions in the genes *rffH* and
327 *rffG* than in the parent TraDIS library (**Fig 4A)**. The gene products RffH and RffG catalyse the
328 same enzymatic reaction and are homologous in sequence to the genes RfbA and RfbB,
329 respectively. However, they form part of different operons and function in separate pathways
330 despite *rffG* being able to complement an RfbB defective strain [47, 48]. This likely explains
331 why *rffH* and *rffG* are not entirely essential in the Δ*surA* background.
332 ECA exists in three forms that all share the same biosynthetic pathway: ECA that is covalently
333 linked to LPS (ECA_{LPS}), covalently linked to diacylglycerol-phosphate (ECA_{PG}), or a cyclic form
334 (ECA_{CYC}) that is localised to the periplasm as opposed to being surface exposed [45, 49]. We
335

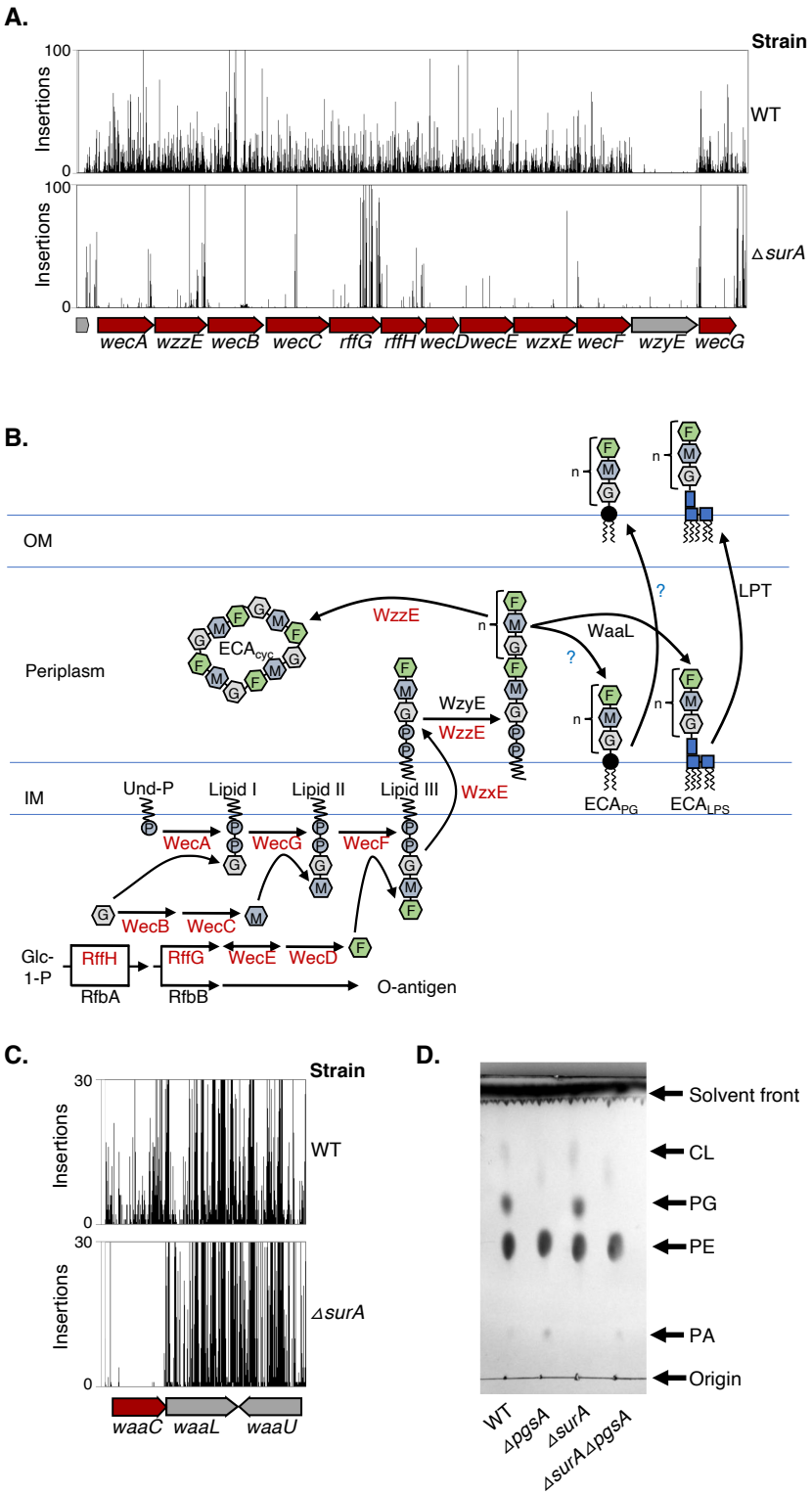

Figure 4 – Synthesis of ECA is essential in the absence of the chaperone SurA

A. Transposon insertions in genes of the ECA biosynthesis pathway in the parent or Δ*surA* mutant TraDIS libraries. Transposon cut-off is set to 100. Essential genes are represented as red arrows. **B.** Schematic representation of the ECA biosynthesis pathway with the names of proteins labelled next to the reaction for which they are responsible. Conditionally essential proteins are labelled in red text. **C.** Transposon insertions in the *waaL* gene in either the parent or Δ*surA* mutant TraDIS libraries. Transposon cut-off is set to 100. **D.** Analysis of phospholipid content in the parent or Δ*surA* mutant with further mutations to disrupt synthesis of the major anionic phospholipids. The Δ*pgsA* *and* Δ*surA*Δ*pgsA* strains are also Δ*lpp*Δ*rcsF*. Phospholipid samples were separated and visualised by TLC using a solvent mixture of methanol/ chloroform/ water with a ratio of 2:2:1.8 before being visualised by phosphomolybdic acid and charring.

382

383 sought to determine which form of ECA is conditionally essential in Δ*surA*. Synthesis of
384 ECA_{LPS} is facilitated by the O-antigen ligase WaaL, which is responsible for attaching the ECA
385 molecule onto the LPS core [50, 51]. However, in the Δ*surA* TraDIS library, the gene *waaL* is
386 non-essential **(Fig 4C)**. This suggests that ECA_{LPS} is not essential in the Δ*surA* mutant. The
387 formation of ECA_{PG} is completed by attachment of linear ECA chains to diacylglycerol by a
388 phosphodiester bond through an unknown mechanism [50, 52]. To determine the essentiality
389 of ECA_{PG} we targeted synthesis of the donor molecule for ECA_{PG}, the phospholipid
390 phosphatidylglycerol [53]. The gene *pgsA* encodes phosphatidylglycerophosphate synthase,
391 which catalyses the first committed step in biosynthesis of phosphatidylglycerol. However, loss
392 of *pgsA* is lethal due to mislocalisation of Braun's lipoprotein, Lpp, to the inner membrane and
393 activation of the Rcs stress system. These issues can be resolved by making an Δ*lpp*Δ*rcsF*
394 mutant before constructing the Δ*pgsA* mutation [54-56]. The Δ*pgsA*Δ*surA*Δ*lpp*Δ*rcsF*
395 quadruple mutant was viably constructed and the absence of phosphatidylglycerol was
396 confirmed by phospholipid extraction and thin layer chromatography **(Fig 4D)**. This confirmed
397 that the phospholipid donor for synthesis of ECA_{PG} is not essential in the Δ*surA* mutant. Lastly,
398 the gene *wzzE* is not required for the production of ECA_{LPS} or ECA_{PG}, but is required for
399 production of ECA_{CYC} [50, 57, 58]. In the Δ*surA* TraDIS library, the gene *wzzE* contained a
400 conditionally essential region indicating that ECA_{CYC} is likely to be the form of ECA that is
401 conditionally essential in a Δ*surA* mutant **(Fig 4A)** [57].
402
403 ***meso*-DAP is essential in the absence of BamB, BamC or BamE**
404 The TraDIS data were searched for conditionally essential genes involved in cell envelope
405 biogenesis pathways other than LPS and ECA biosynthesis. The gene *dapF* was identified as
406 conditionally essential in Δ*bamB* and Δ*bamC* with visual inspection indicating decreased
407 insertions in *dapF* in Δ*bamE* **(Fig 5A)**. This was particularly surprising considering the lack of
408 strong phenotypes in the Δ*bamC* background **(Fig 1)**. DapF converts LL-diaminopimelate (LL-
409 DAP) to *meso*- diaminopimelate (*meso*-DAP), which is then either decarboxylated to produce

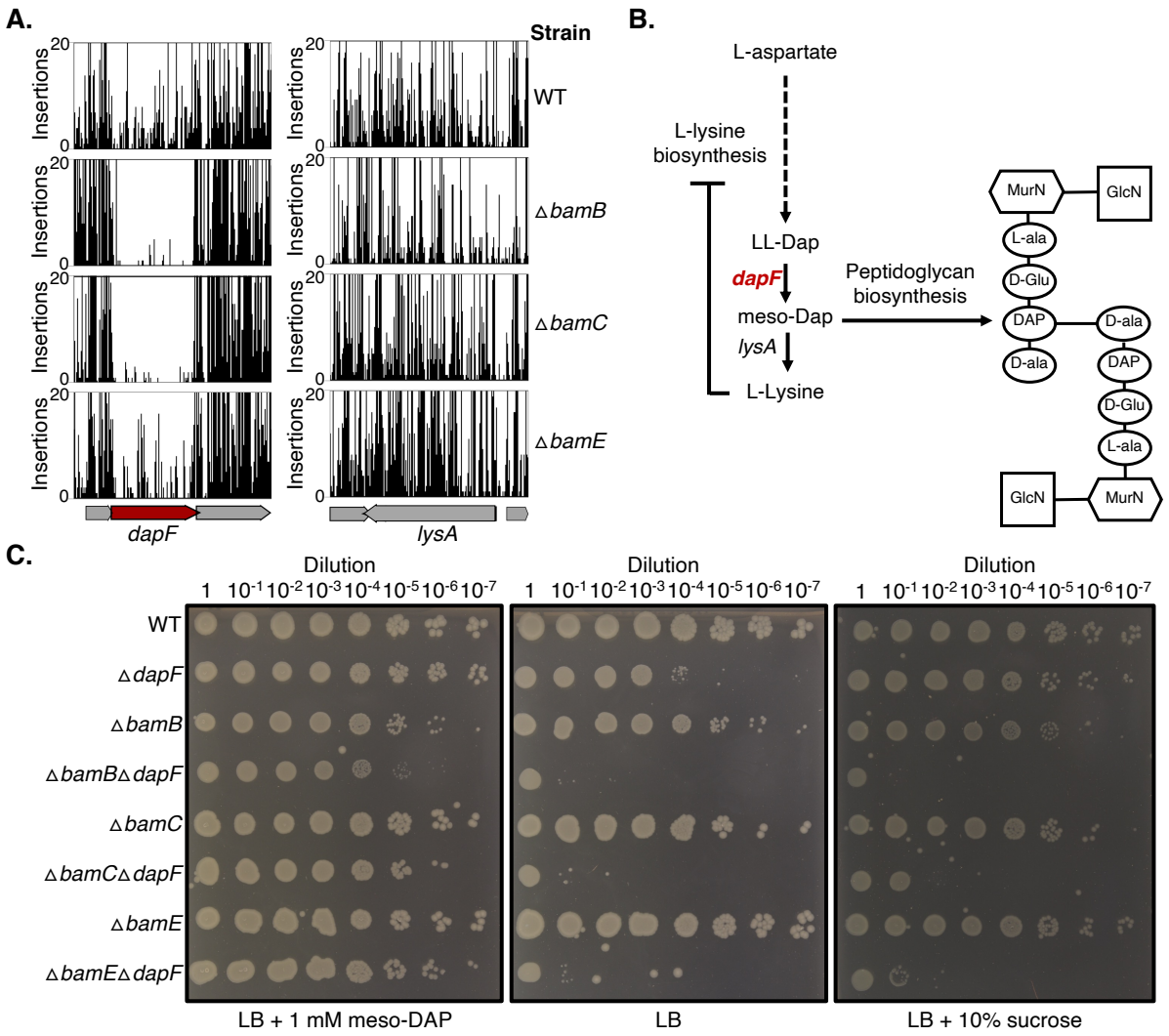

Figure 5 – *meso*-DAP containing peptidoglycan is essential in the absence of Bam accessory lipoproteins

A. Transposon insertions in the genes *dapF* and *lysA* in the parent or Δ*bamB,* Δ*bamC,* Δ*bamE* mutant TraDIS libraries. Transposon cut-off is set to 20. Essential genes are represented as red arrows. **B**. Schematic representation of the L-lysine biosynthesis pathway with the names of proteins labelled next to the reaction for which they are responsible. Conditionally essential proteins are labelled in red text. A schematic structure of *E. coli* peptidoglycan is shown with the site of *meso*-DAP incorporation shown. **C.** Efficiency of plating assay showing survival of the Δ*dapF,* Δ*bamB,* Δ*bamC,* Δ*bamE,* Δ*dapF*Δ*bamB,* Δ*dapF*Δ*bamC, or* Δ*dapF*Δ*bamE* mutants grown on LB with or without 1 mM *meso*-DAP or 10 % sucrose. Cells were grown overnight in LB supplemented with 1 mM *meso*DAP before being normalised to OD_{600} = 1.00 and serially diluted 1:10 before 2 μl was spotted on agar plates and incubated at 37°C overnight.

423 L-lysine by the enzyme LysA or is used in biosynthesis of peptidoglycan [59, 60]. The gene
424 *lysA* was non-essential in all strains tested, suggesting the essentiality of *dapF* in these
425 mutants is due to the requirement for *meso*-DAP in peptidoglycan **(Fig 5A and 5B)**. To validate
426 the genetic interaction between Δ*dapF* and components of the Bam complex, the *dapF* gene
427 was knocked out in the BW25113 parent strain, Δ*bamB,* Δ*bamC* or Δ*bamE* mutants. The
428 double knockouts were selected in the presence of externally supplied *meso*-DAP, which
429 alleviated the loss of *dapF*. Cells were then grown in liquid media in the presence of *meso*-
430 DAP before being serially diluted in un-supplemented media and assayed for survival in the
431 presence or absence of *meso*-DAP by efficiency of plating assay. All strains grew equally as
432 well as the parent on LB agar supplemented with 1 mM *meso*-DAP, except for Δ*bamB*Δ*dapF*
433 which showed a minor decrease in CFU and colony size **(Fig 5C)**. However, in the absence
434 of *meso*-DAP the single Δ*dapF* mutant demonstrated a decrease in survival and the double
435 mutants were not viable **(Fig 5C)**. Lastly, considering that loss of DapF will lead to a weaker
436 peptidoglycan layer due to decreased crosslinks, we sought to negate the synthetic-lethal
437 phenotype by growth in the presence of sucrose as an osmoprotectant [61, 62]. Unexpectedly,
438 while the presence of 10% sucrose enabled survival of the single *dapF* mutant to levels
439 comparable to the parent, this was insufficient to restore growth of the double mutant **(Fig 5C)**.
440 This data demonstrates that peptidoglycan structure is of increased importance in the absence
441 of full Bam complex activity and that this may not simply be due to structural support for the
442 envelope.
443
444 **Regulation of DNA replication initiation is disrupted in the absence of BamB**
445 Our TraDIS experiment identified that in the Δ*bamB* dataset three KEGG pathways were
446 significantly enriched: “Homologous recombination”, “Mismatch repair” and “DNA replication”.
447 Bacterial DNA replication is mainly regulated at the initiation step by DnaA **(Fig 2A and 6A)**.
448 The ATP-bound form of this protein binds to DnaA boxes present at the chromosomal origin
449 of replication (*oriC*), with both high and low affinity, and directs replisome assembly [63].
450 Briefly, DnaA-ATP forms an oligomeric complex that facilitates unwinding of the DNA strands,

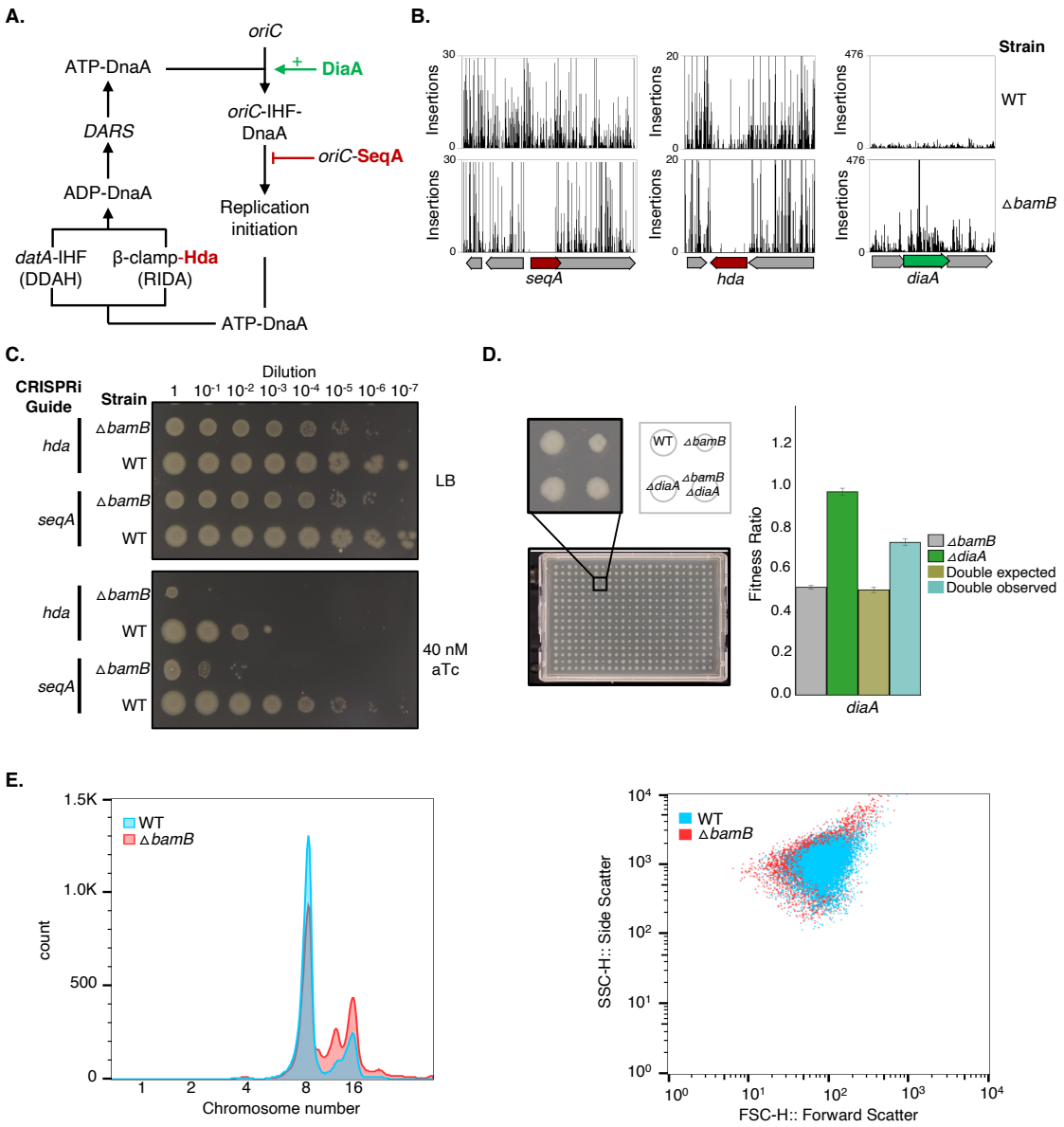

Figure 6 – Loss of BamB leads to changes in DNA replication control
A. Schematic representing DNA replication control in *E. coli*. DiaA stimulates initiation at the origin of replication, *oriC*, by DnaA. SeqA prevents premature reinitiation of replication. Hda acts together with the β-sliding clamp to hydrolyse ATP-bound DnaA by regulatory inactivation of DnaA (RIDA). This can also occur through *datA*-dependent DnaA-ATP hydrolysis (DDAH). **B.** Transposon insertions in the genes *hda*, *seqA* and *diaA* in the parent or Δ*bamB* mutant TraDIS libraries. Conditionally-essential genes are represented as red arrows and genes that increase fitness are in green. **C.** Efficiency of plating assay showing survival of the parent dCas9 expressing strain LC-E18 (WT) or Δ*bamB* mutant derivatives carrying the pSGRNA plasmid, which encodes CRISPRi guide RNA targeting either *seqA* or *hda*. Cells were grown on LB with or without 40 nM anhydro-tetracycline (aTc) to induce guide RNA expression. **D.** The *E. coli* BW25113 parent strain, single, or double Δ*bamB* and Δ*diaA* mutants were spotted on LB agar in 384-well format, in triplicate, and grown overnight at 37°C before being imaged. Fitness was calculated based on colony size and fitness ratios generated relative to the WT parent. **E.** Flow cytometry of *E. coli* LC-E18 cells grown in LB followed by replication run-out assay. Forward scatter and side scatter are plotted with WT cell data indicated in blue and Δ*bamB* data points in red. Fluorescence is plotted and represents chromosomal content for each cell with chromosome numbers for each peak marked

470 which in turn enables assembly of the replisome: the complex responsible for replication of
471 the bacterial chromosome. In *E. coli,* DnaA binding to its cognate DnaA boxes is modulated
472 by regulatory proteins. Negative regulation is achieved by two proteins. The protein SeqA
473 sequesters newly replicated origins, preventing premature reinitiation of replication [64-66].
474 The Hda protein works together with the β-sliding clamp to stimulate ATP hydrolysis of DnaA-
475 ATP, which in the ADP-bound form is unable to promote initiation of DNA replication [64-68].
476 Positive regulation is facilitated by the DnaA initiator-associating factor, DiaA, which directly
477 interacts with the N-terminal domain of DnaA to stimulate initiation at *oriC* [69, 70].
478 Analysis of the TraDIS data identified the genes *holC, holD, matP, seqA* and *hda* as
479 conditionally essential in the Δ*bamB* mutant **(Table S1)**. Within this set of genes, we chose to
480 focus on those with the clearest conditional essentiality from the TraDIS data, *hda* and *seqA.*
481 Insertions within the negative regulator encoding genes, *seqA* and *hda*, led to decreased
482 survival of Δ*bamB*. In contrast, increased fitness of Δ*bamB* was observed for cells containing
483 disruptions of the positive regulator gene *diaA* **(Fig 6B)**. We confirmed the findings regarding
484 the negative regulators by using CRISPRi. The *bamB::aph* allele was transferred into the
485 dCas9 encoding strain *E. coli* LC-E18 and the kanamycin resistance marker was removed.
486 The pSGRNA plasmid was used to express guide RNA targeting the *seqA* or *hda* genes in
487 either the parent or Δ*bamB*. Expression of guide RNA targeting the *seqA* and *hda* genes led
488 to significantly decreased survival of Δ*bamB* when compared to the parent strain, therefore
489 confirming the observations made from TraDIS **(Fig 6C)**. The positive genetic interaction
490 between *bamB* and *diaA* was confirmed by measuring fitness of the Δ*bamB*Δ*diaA* mutant
491 compared to both single deletion mutants. Fitness of the double mutant was greater than the
492 expected fitness for this strain **(Fig 6D)**.
493 Considering that loss of negative regulators of DNA replication initiation led to decreased
494 fitness of Δ*bamB*, and loss of the positive regulator increases fitness, we hypothesised that
495 the Δ*bamB* mutant may already have defective replication control. Therefore, we compared
496 chromosomal content of the wild-type and Δ*bamB* strain by using an established replication

497 run-out assay [71]. Both strains were grown to early exponential phase under conditions
498 supporting fast cell growth (LB + 0.2% glucose), when cells contain multiple replicating
499 chromosomes. We reasoned that dysfunction of replication control is usually exacerbated
500 when cells grow with overlapping replication rounds. Next, cells were collected and treated
501 with rifampicin to inhibit further rounds of DNA replication initiation, and with cephalexin to
502 prevent cell division. Fixed cells were stained for DNA content with Sytox Green and analysed
503 by flow cytometry. The comparison of chromosomal copy number revealed a higher proportion
504 of cells with 16 chromosome copies for the Δ*bamB* mutant, which implies that initiation of
505 replication occurs earlier during the cell cycle in this strain relative to the parent. Strikingly, a
506 population of Δ*bamB* cells also displayed a number of chromosomes deviating from the
507 normally observed 2^n, as manifested by an additional peak between the 8 and 16 chromosome
508 peaks. This is a hallmark of asynchronous DNA replication events, when not all replication
509 origins in the cell fire simultaneously **(Fig 6E, S8-10)**. Analysis of the other Bam-accessory
510 lipoprotein gene mutants and Δ*skp* by replication run-out assay revealed no significant
511 changes from the parent pattern **(Fig S11)**. Therefore, our results suggest that *E. coli* over-
512 initiates DNA replication in the absence of BamB. This is consistent with the observations that
513 Δ*bamB* cells are more fit if they lose the positive regulator of DNA replication, DiaA, but have
514 decreased fitness in the absence of the negative regulators SeqA and Hda.
515

516 **OMP trafficking protein conservation varies throughout Gram-negative bacteria**

517 The data presented here demonstrate that in *E. coli,* the Bam-associated proteins likely have
518 specialised functions that are potentially coordinated with LPS structure, the presence and
519 form of ECA, peptidoglycan biogenesis and DNA replication control. Considering these
520 results, we revisited the evolutionary conservation of Bam complex subunits and the
521 periplasmic chaperone pathway proteins [72]. Reference genomes for a diverse range of
522 Gram-negative bacterial representative strains were used to search for sequences coding the
523 Bam complex subunits (as observed in *E. coli*) or the chaperone pathway proteins SurA, Skp

524 and DegP. A combination of Prokka annotation, hmmsearch, SignalP 6.0 [73] and manual
525 curation were used to generate a neighbour joining tree with a heat map of gene counts in
526 each organism **(Fig 7)**. While we found broad conservation of all query proteins within the
527 gamma- and beta-proteobacteria, there are some notable exceptions. The BamB and BamC
528 lipoproteins are not conserved within two species of the aphid endosymbiont *Buchnera*
529 *aphidicola* and the data confirm previous unpublished observations that a strain of *B.*
530 *aphidicola*, (subspecies *Baizongia pistaciae*) appears to have entirely lost genes encoding the
531 Bam complex [74]. Likely this is due to the strain containing only a few OMPs, therefore no
532 longer requiring a dedicated OMP assembly machinery.
533 Outside of the gamma- and beta-proteobacteria, requirement for the Bam-associated proteins
534 appears to be diverse. The lipoproteins BamB and BamC are largely absent in the alpha-
535 proteobacteria, and the epsilon-proteobacteria only encode the core components BamA and
536 BamD, demonstrating reductive evolution. This minimalist form of the Bam complex is
537 sufficient for OMP insertion, which is likely due to reduced β-barrel complexity as observed in
538 *Helicobacter pylori* [75] **(Fig 7)**. While there is diversity in the presence or absence of these
539 proteins in the organisms analysed, multiple copies of some components were also identified.
540 We found that *Pseudomonas putida* encodes two copies of BamA, BamE and SurA. Outside
541 of the gamma-proteobacteria there are numerous examples of species encoding multiple
542 copies of BamA, particularly within the alpha-proteobacteria, such as the plant pathogen
543 *Agrobacterium tumefaciens* **(Fig 7)**. These copies may play specialised roles in folding and
544 inserting specific cargo, or they may alleviate an increased requirement for OMP insertion in
545 these organisms. Taken together, the diverse range of Bam complex subunit compositions
546 within Gram-negative bacteria support the hypothesis that the Bam-associated proteins likely
547 play specialised roles that vary in each organism.

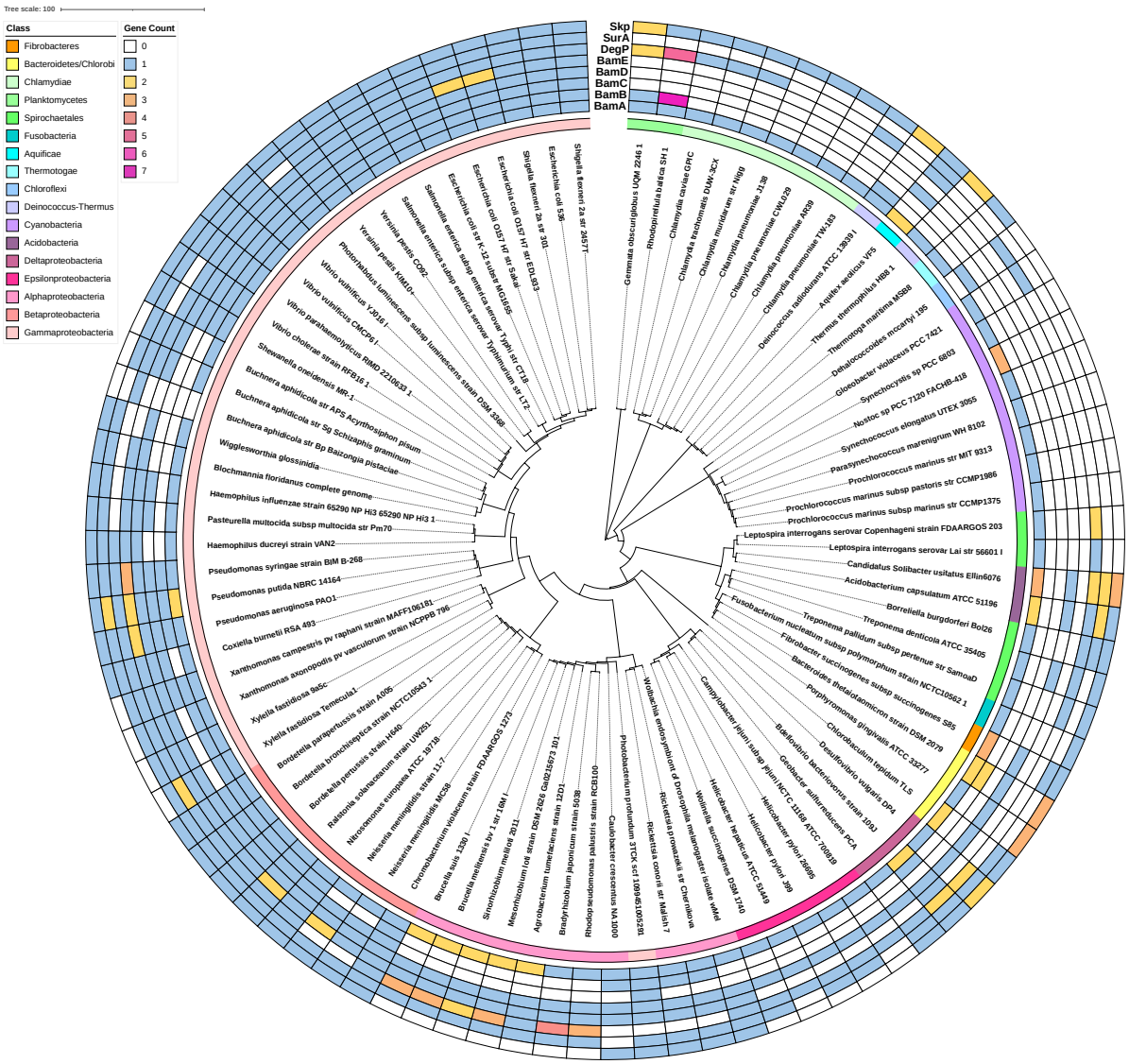

Figure 7 – Conservation analysis of Bam-associated proteins in Gram-negative bacteria
Conservation of the BamB, BamC, BamE, SurA, DegP and Skp proteins among key Gram-negative bacterial species represented by a presence/absence map plotted onto a phylogenetic tree generated with iTOL [76]. Gene count in each species is represented by coloured boxes.

555 **Discussion**

556 The Bam complex has been identified as a significant unrealised target for new antimicrobials,
557 with several new inhibitors of this essential outer membrane biogenesis machine being
558 identified recently [77, 78]. However, despite this focus as an important new avenue for drug
559 discovery, and recent advances in understanding the mechanism by which the Bam complex
560 folds and inserts OMPs into the outer membrane [79, 80], we still do not fully understand the
561 roles of the Bam-associated proteins in *E. coli*. We also do not understand why the complex
562 appears to be modular, with subunits being differentially conserved throughout Gram-negative
563 bacteria as shown through our analysis and those done previously **(Fig 7)** [72]. Constituent
564 parts of the outer membrane such as phospholipid species, type of LPS, O-antigen, ECA,
565 lipoprotein content, and variety/flux of the unfolded OMP proteins can vary across bacterial
566 species [81, 82]. Such variation would likely result in significant differences in the biophysical
567 constraints of the membrane environment in which the Bam complex must operate. In addition,
568 there is likely to be differing requirements for the chaperone pathway proteins depending on
569 the pool of client OMPs. Considering that Skp and SurA have been shown to act on different
570 unfolded states of OmpC, with Skp likely being more important during stress conditions, the
571 environmental conditions experienced by each species could also dictate the requirement for
572 each OMP chaperone [6]. Together, this strongly suggests that each accessory lipoprotein is
573 likely to have specialised functions and that the chaperone proteins are unlikely to be truly
574 functionally redundant. This is supported by our phenotypic profiling of knockout strains.
575 Should each of the accessory lipoproteins merely contribute to overall activity of the Bam
576 complex, and if there is true redundancy in the chaperone pathway, then we would expect that
577 the knockout strains should phenocopy each other. However, we found this not to be the case
578 **(Fig 1)**. Our TraDIS analysis also supports this conclusion as we saw a large number of unique
579 conditionally essential genes for each mutant **(Fig 2)**.

580

581 *Role of the outer membrane lipid environment for OMP insertion*

582 The Bam complex must function within the constraints of the outer membrane lipid

583 environment, therefore OMP biogenesis is likely to be affected by changes to outer membrane
584 lipids. Indeed, we found conditional essentiality between genes involved in LPS inner core
585 biogenesis and either *bamB*, *surA* or *degP*. Complete truncation of the LPS inner core by
586 disruption of the last enzyme in the heptose biosynthesis pathway has previously been
587 demonstrated to increase membrane fluidity and lead to decreased Bam complex activity [40].
588 We confirmed this observation and further demonstrate that the changes to membrane fluidity
589 are of graded severity relating to the severity of LPS inner core truncation. This in turn leads
590 to a graded impact on Bam complex activity **(Fig 3)**. The Δ*bamB,* Δ*surA* and Δ*degP* knockout
591 strains have the most severe phenotypes within the set of strains tested here (**Fig 1)**. Also,
592 loss of BamB, SurA or DegP each leads to OMP assembly defects, decreased numbers of
593 folded OMPs in the outer membrane, and accumulation of unfolded OMPs in the periplasm
594 [9, 26, 83-85]. We hypothesise that the negative effect of increased membrane fluidity on the
595 Bam complex in combination with decreased levels of OMP assembly in the absence of BamB,
596 SurA or DegP leads to OMP assembly levels that are too low to sustain cell viability. This is of
597 particular significance when considering the variation in LPS structure seen between different
598 strains, and the LPS modifications available, which could affect the level of Bam activity and
599 influence the conservation of each Bam-associated protein [81, 82].
600
601 *A role for ECA_{cyc} in amelioration of periplasmic protein folding stress?*
602 The carbohydrate antigen ECA consists of three repeating sugars, is widely conserved
603 amongst the *Enterobacterales*, and is produced in three forms that are either surface exposed
604 (ECA_{LPS} and ECA_{PG}) or periplasmically localised (ECA_{CYC}). The invariant nature of the antigen
605 suggests it has an important undiscovered function, however the role of ECA in outer
606 membrane biology remains unknown [49]. We identified that ECA biogenesis becomes
607 essential in the absence of the chaperone SurA **(Fig 4A)**. Production of ECA requires the lipid
608 carrier undecaprenyl phosphate (Und-P), which is limited in the cell and utilised in numerous
609 metabolic reactions including the production of peptidoglycan, capsule, O-antigen and
610 membrane-derived oligosaccharides. Disruption of ECA biogenesis can cause stress on these

611 other pathways due to Und-P sequestration in ECA dead-end intermediates [49, 57, 86].
612 However, the first gene in the ECA pathway is conditionally essential in the absence of SurA
613 **(Fig 4A)**, therefore the effects are unlikely due to stress on the Und-P pool. Instead, we
614 showed that the periplasmically localised form, ECA_{cyc}, is essential in the absence of SurA
615 **(Fig 4)**. It is possible that ECA_{cyc} might help stabilise the outer membrane of a Δ*surA* mutant,
616 as it has been shown to suppress the envelope permeability defect of a Δ*yhdP* mutant.
617 However, the molecular details of this suppression are yet to be discovered [57]. Alternatively,
618 ECA_{cyc} could be performing a chaperone function directly, however this would require *in vitro*
619 assays of protein aggregation with purified products for proof.
620
621 *Coordination of OMP biogenesis with peptidoglycan biosynthesis*
622 To ensure successful cell growth and division, activity of the Bam complex must be
623 coordinated with biogenesis of the peptidoglycan layer. Our TraDIS analysis identified that in
624 the Δ*bamB,* Δ*bamC* and Δ*bamE* mutants, the gene *dapF* was essential **(Fig 5A)**. The DapF
625 enzyme is responsible for synthesis of the peptidoglycan stem-peptide component *meso*-DAP.
626 The single and double mutants could be rescued by exogenous *meso*-DAP, however only the
627 single *dapF* mutant could be rescued by the osmo-protectant sucrose, which is sufficient to
628 allow survival during disruption of peptidoglycan biogenesis **(Fig 5B)** [61]. Loss of *meso*-DAP
629 in the single *dapF* mutant leads to accumulation of LL-DAP, which is incorporated into
630 peptidoglycan and leads to decreased crosslinking [59, 62]. In the Δ*dapF* mutant the
631 peptidoglycan layer would be able to withstand less mechanical load due to decreased
632 crosslinking. This decreased mechanical strength, in combination with the reduced capacity
633 for load bearing by the outer membrane in the Bam complex mutants, means that the cells
634 are unlikely to withstand osmotic stress [87]. However, while this may be true for Δ*bamB* and
635 Δ*bamE* mutants, there are no strong phenotypic effects for Δ*bamC* (**Fig 1)** [88]. Also, the loss
636 of BamC has only a slight effect on the membrane permeability barrier, no detectable changes
637 to the outer membrane proteome, and no effect on OMP folding in an *in vitro* assay [9, 89].

638 Consequently, the synthetic lethality between *dapF* and *bamC* is unlikely to be due to osmotic
639 stress tolerance, as could be the case for the other mutants.
640 It has recently been demonstrated that the Bam complex preferentially inserts OMPs at the
641 cell division site and that this is coordinated by interaction with the peptidoglycan layer [90].
642 While all of the Bam complex proteins were shown to interact with peptidoglycan *in vitro*, only
643 BamA and BamC were found to interact with peptidoglycan in whole cells when analysed by
644 crosslinking and pull-down assays [90]. Considering the interaction of mature peptidoglycan
645 with BamC and the altered peptidoglycan structure in the Δ*dapF* strain [59, 62], we
646 hypothesise that BamC might facilitate coordination between the Bam complex and
647 peptidoglycan biosynthesis, however this requires further investigation.
648
649 *Link between OMP biogenesis and DNA replication control*
650 Not only must envelope biogenesis processes be coordinated with each other, but synthesis
651 of the envelope must be coordinated with cell growth and cell division. Experimental evidence
652 suggests that both DNA replication control [91, 92] and the rate of cell surface synthesis are
653 coupled to cell volume [93]. This provides the rationale for existence of mechanisms that
654 modulate DNA replication rate in response to cell envelope synthesis perturbation. Here we
655 demonstrated that in the absence of BamB, cells over-initiate DNA replication and that
656 synchrony of replication initiation at multiple origins is compromised **(Fig 6E)**. Also, our
657 phenotypic screen revealed that Δ*bamB* has increased fitness at sub-optimal growth
658 temperatures. This would lead to slower growth, a factor that is known to alleviate some DNA
659 replication control defects, such as those arising from loss of SeqA [64]. In addition, we found
660 that the Δ*bamB* mutant is sensitive to hydroxyurea, which specifically inhibits ribonucleotide
661 reductase and leads to depletion of the cellular dNTPs pool, replication fork arrest and
662 genomic instability **(Fig 1)** [94, 95]. Similarly to Δ*bamB*, mutants that over-initiate replication,
663 such as *seqA* mutants, are also sensitive to hydroxyurea [96].

664 Led by our TraDIS results, we confirmed that *seqA* and *hda* are essential in the Δ*bamB* mutant
665 **(Fig 6)** and that this is likely due to over-initiation of DNA replication, which can be caused by
666 all three of these mutations [64, 66, 97]. SeqA is required to prevent premature re-initiation of
667 replication through sequestration of newly replicated GATC sites within oriC, whereas Hda
668 prevents re-initiation of replication through regulatory inactivation of DnaA (RIDA), in
669 combination with the β-sliding clamp of DNA polymerase [64, 98]. Interestingly, we also
670 identified that two components of the β-sliding clamp loader complex, HolC and HolD, become
671 essential in the Δ*bamB* mutant **(Table S1)**. These proteins contribute towards activity of the
672 clamp loader. Therefore, the synthetic lethality could be due to decreased RIDA and over-
673 initiation of DNA replication, as observed for the *hda* mutant [68, 99].
674 This is the first link between the Bam complex and DNA replication control, however links
675 between the envelope and DNA replication have been observed previously. In order to initiate
676 DNA replication, the DnaA protein must be in the ATP-bound form and regeneration of DnaA-
677 ATP from the ADP-bound form is facilitated by interaction with phospholipids. [100, 101]. DNA
678 replication control and envelope biogenesis are also linked by the SeqA protein, which has
679 been associated to the purified outer membrane fraction in a cell-cycle dependent manner,
680 however the mechanism remains unclear [102]. In addition, disrupted origin/terminus ratios in
681 *seqA* mutant strains are suppressed by mutations in the *waaG, waaQ* and waa*P* genes, which
682 are responsible for addition of the outer core of LPS, heptose III addition to the inner core and
683 phosphorylation of heptose II of the LPS inner core, respectively [81, 103]. Interestingly, the
684 Δ*bamB* mutant is also sensitive to changes in membrane fluidity brought about by LPS
685 modifications that map to the inner core **(Fig 3)**.
686 We also identified that insertions in the *diaA* gene, which encodes a positive regulator of DNA
687 replication initiation, can suppress Δ*bamB*. The *diaA* gene is part of a conserved four gene
688 cluster that also encodes LpoA - a regulator of peptidoglycan biogenesis, YraN - a protein of
689 unknown function, and DolP - a cell-division site localised outer membrane lipoprotein shown
690 to interact with the Bam complex [104, 105]. The genes in this cluster all appear to be linked

691 to regulating cellular growth processes such as peptidoglycan biogenesis, OMP insertion into
692 the outer membrane and DNA replication. This is of particular interest considering our data
693 demonstrate potential coordination of these processes, which is essential to ensure efficient
694 growth and survival during cell division.
695 Together, our data demonstrate that the Bam-associated proteins have specialised roles in
696 the cell and highlights potential future targets to understand these roles. We provide further
697 evidence that OMP transport, folding and insertion is affected by, and potentially coordinated
698 with, peptidoglycan and LPS structure. We also show that Bam function is correlated with DNA
699 replication control and highlight the BamB lipoprotein, outer membrane fluidity and LPS
700 structure as a potential route through which this could occur. This provides a strong direction
701 for further study to understand this coordination.
702

703 **Acknowledgments**

704 This work was supported by a UKRI Future Leaders Fellowship [MR/V027204/1] and a
705 Springboard Award [SBF005\1112] to Manuel Banzhaf. The work was also funded by the
706 National Science Centre Poland [UMO-2014/13/B/NZ2/01139] (awarded to Monika
707 Glinkowska), the KAUST baseline fund [BAS/1/1108-01-01] awarded to Danesh
708 Moradigaravand who is a member of the KAUST Smart-Health initiative, and the EU ITN
709 Train2Target [721484] that funded training of Kara Staunton.

710 **Supplementary figures**

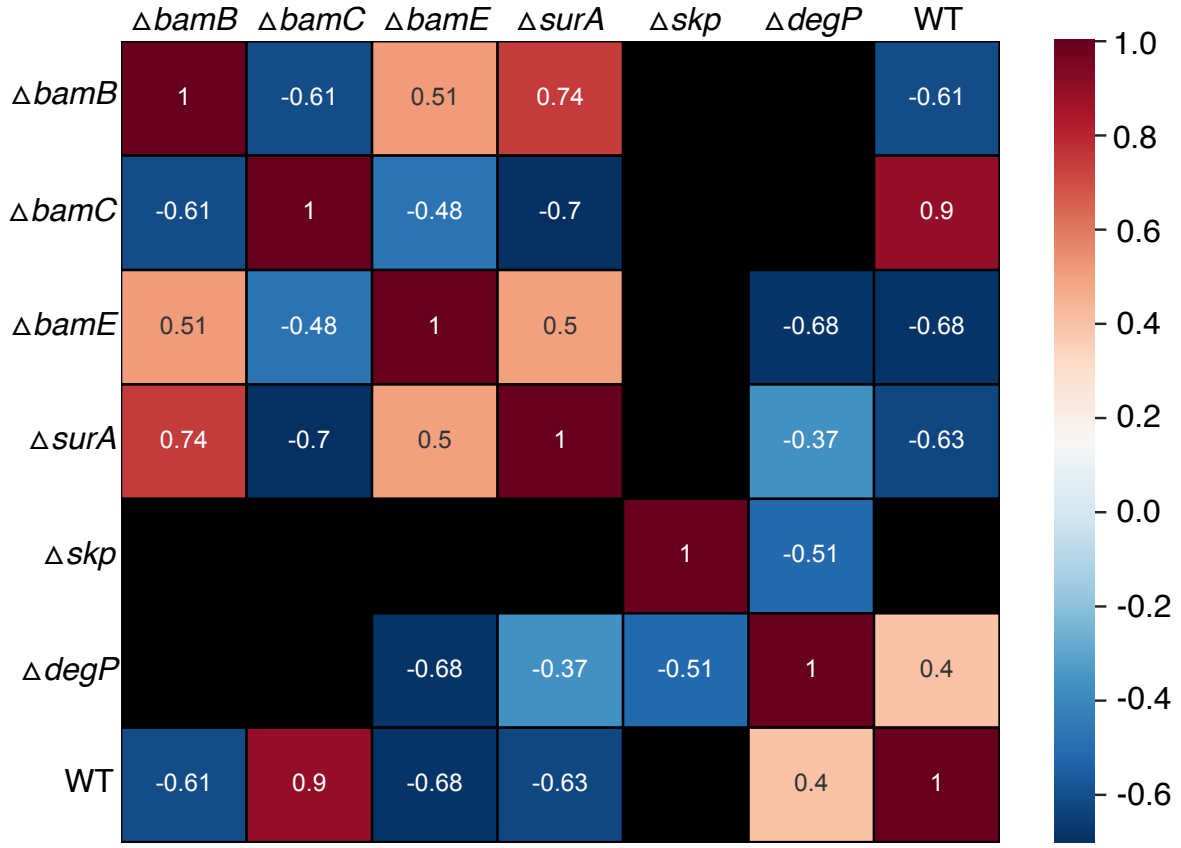

711

712 **Figure S1 – Correlation of phenotypic profiles**
713 Heatmap of Pearson correlation coefficients for each pair of strain phenotypic profiles.
714 Correlation of fitness ratios for each strain was assessed by calculating the Pearson
715 correlation coefficient for averaged fitness scores across replicates using Python before being
716 plotted as a heatmap. Black squares indicate a p-value ≥0.05 meaning the correlation
717 coefficient achieved was not statistically significant.

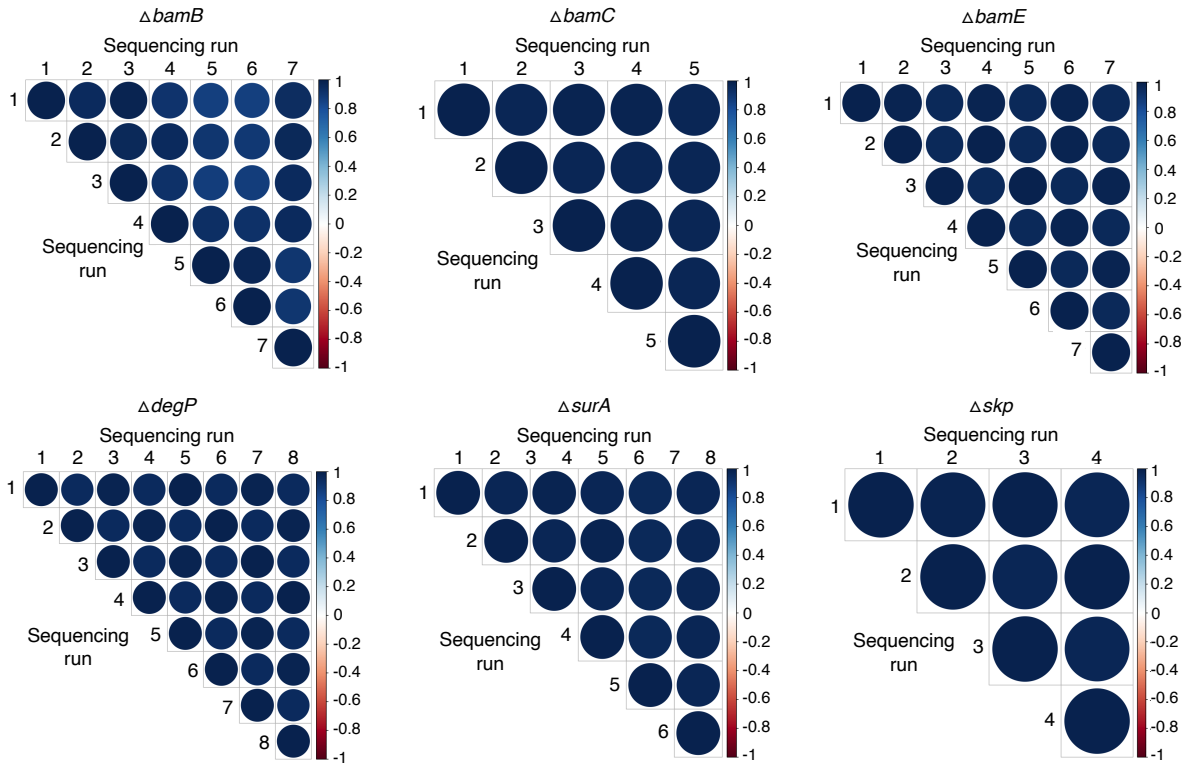

Figure S2 – Reproducibility across TraDIS library sequencing runs
Correlogram of insertion indexes between individual sequencing runs for each TraDIS library. The colour and size of the bubbles correspond to the strength of the Pearson correlation coefficient between the indices for the same genes across the runs. The blue colour represents positive correlation.

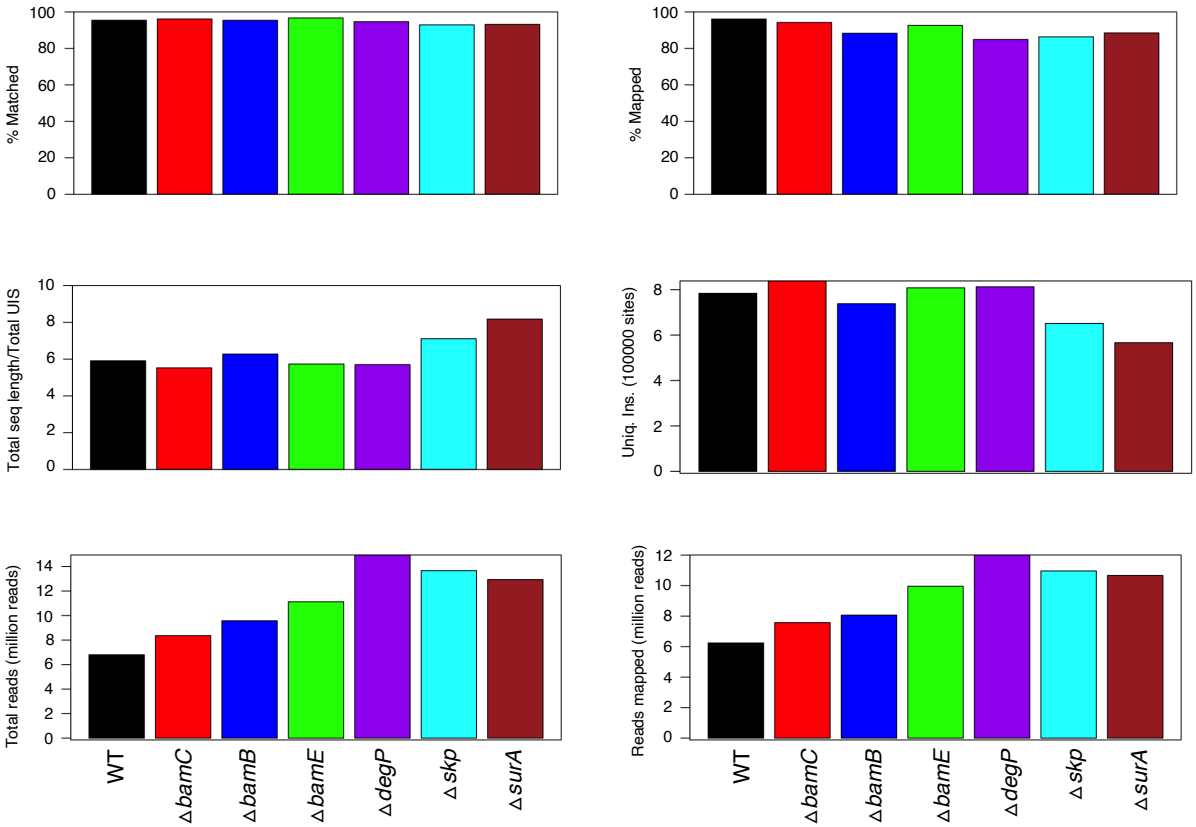

Figure S3 – Transposon library construction metrics
TraDIS library construction metrics showing the percentage of sequencing reads that matched the transposon tag and that mapped to the chromosome. Total sequencing length as a function of total unique insertion sites, the total number of unique insertion sites for each sample, total number of sequencing reads, and the number of reads that mapped are also shown.

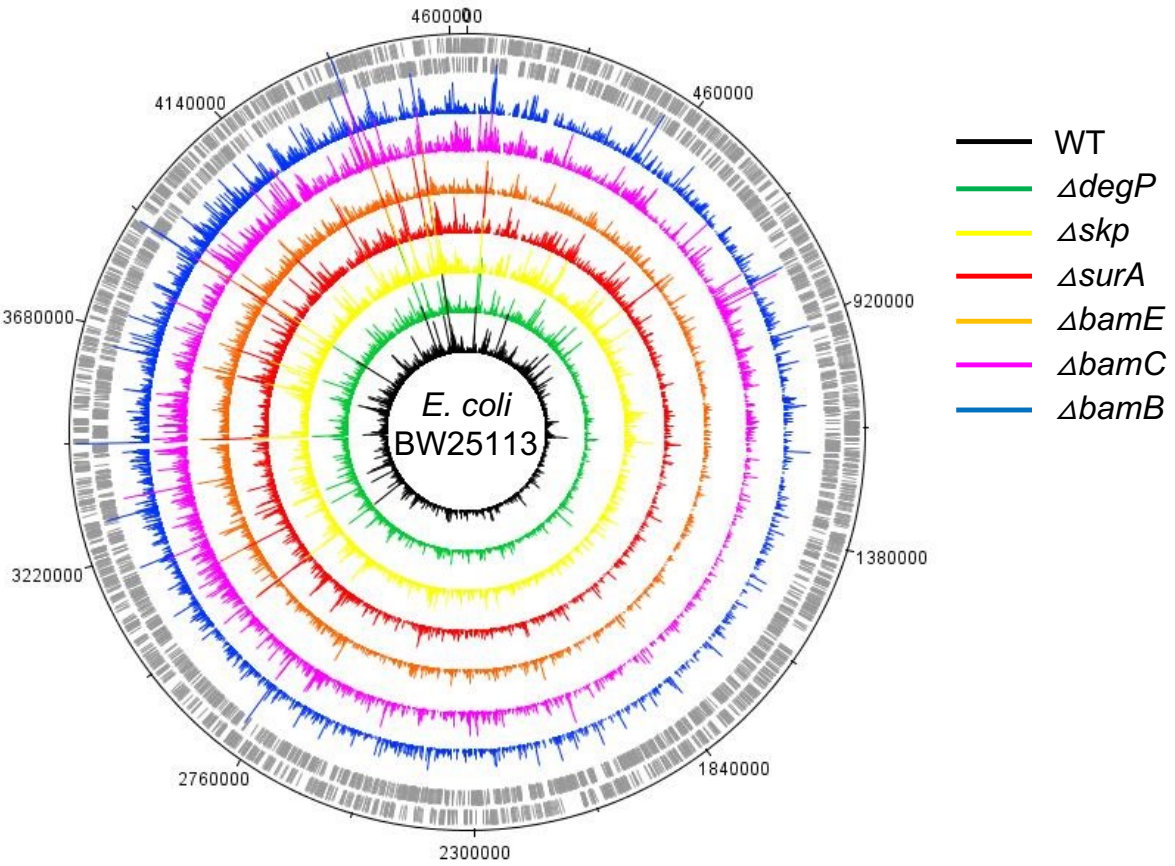

Figure S4 – Circular plots of transposon insertion density in TraDIS libraries. Circular plot of transposon insertion sites in the parent BW25113 (WT), Δ*degP,* Δ*skp,* Δ*surA,* Δ*bamE*, Δ*bamC*, Δ*bamB* TraDIS libraries, listed from innermost tracks outwards, generated using DNAPlotter. The outermost track marks the BW25113 genome in base pairs with the inner grey bar tracks corresponding to sense and antisense CDS.

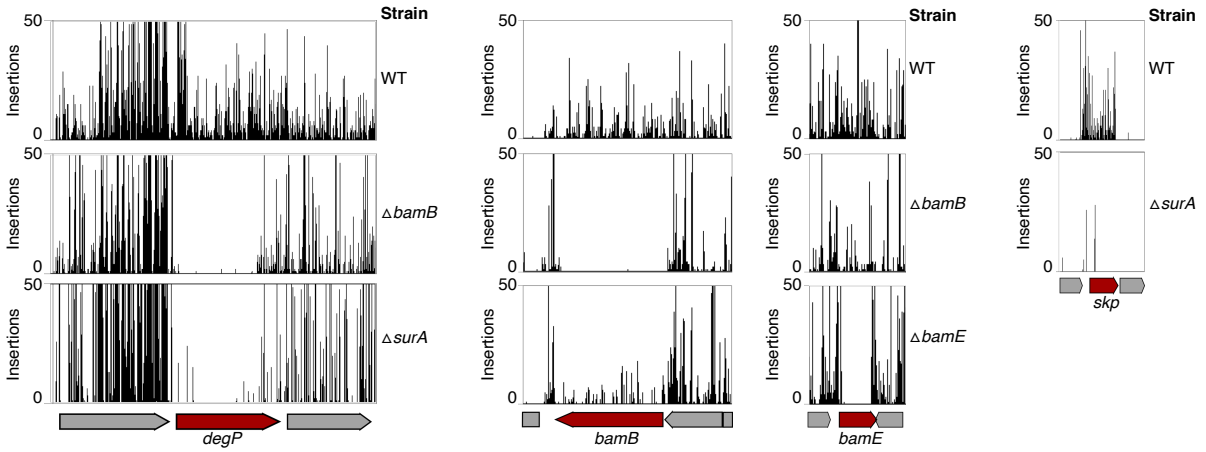

Figure S5 – Examples of known synthetic lethal interactions
Transposon insertions in the genes *degP*, *skp*, *bamB* or *bamE* in the WT parent strain, Δ*bamB*, or Δ*surA* mutant TraDIS libraries. Conditionally-essential genes are represented as red arrows, non-essential genes are represented by grey arrows. Transposon cut-off is set to 50.

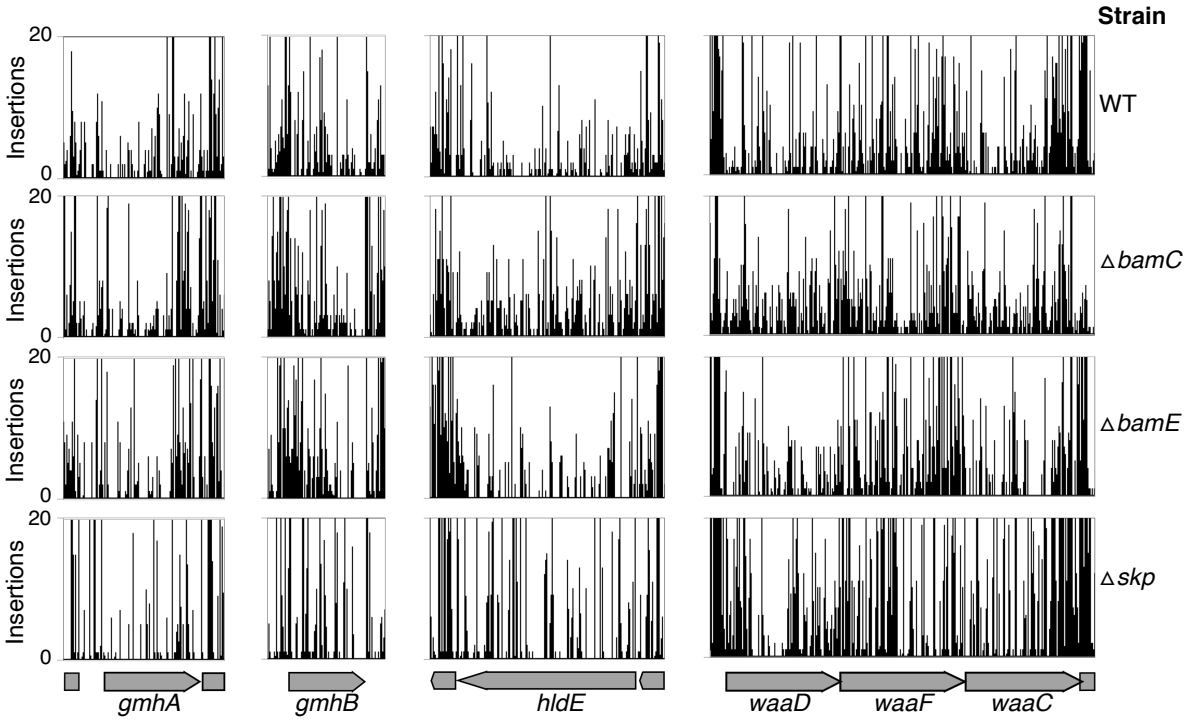

742

743 **Figure S6 – Transposon insertions in genes required for heptose biosynthesis in the**
744 **Δ*bamC*, Δ*bamE* and Δ*skp* TraDIS libraries**
745 Transposon insertions in the genes *gmhA*, *gmhB*, *hldE, waaD, waaC,* and *waaF* in the parent,
746 Δ*bamC,* Δ*bamE* and Δ*skp* TraDIS libraries. Transposon cut-off is set to 20. Essential genes
747 are represented as red arrows and non-essential genes are represented by grey arrows.

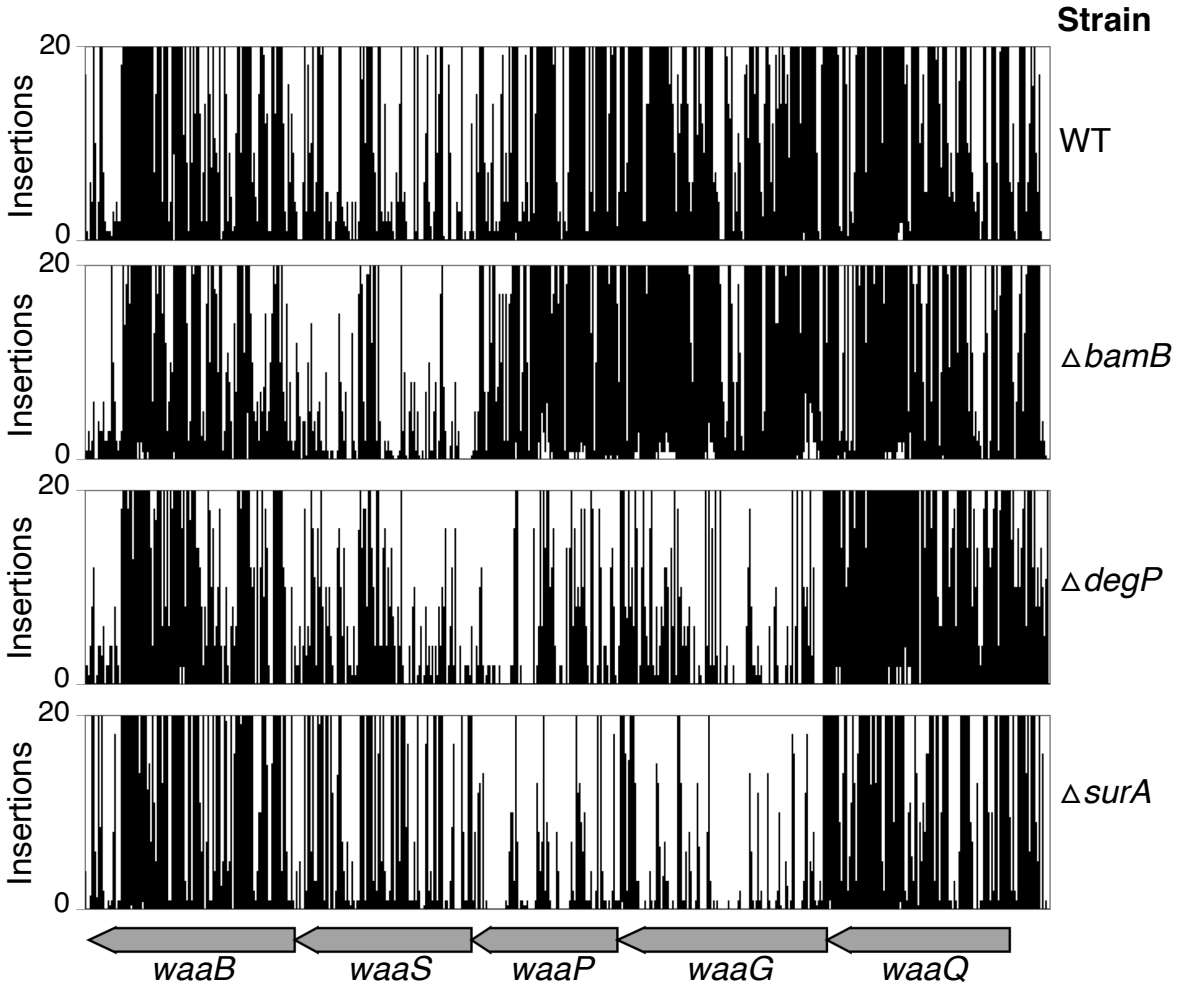

748

749 **Figure S7 – Transposon insertions in the *waaG* and *waaP* genes in the WT, Δ*bamB,***
750 **Δ*degP* and Δ*surA* TraDIS libraries**
751 Transposon insertions in the genes *waaB, waaS, waaP, waaG* and *waaQ* in the parent,
752 Δ*bamB,* Δ*degP* and Δ*surA* TraDIS libraries. Transposon cut-off is set to 20. Genes are
753 represented by grey arrows.

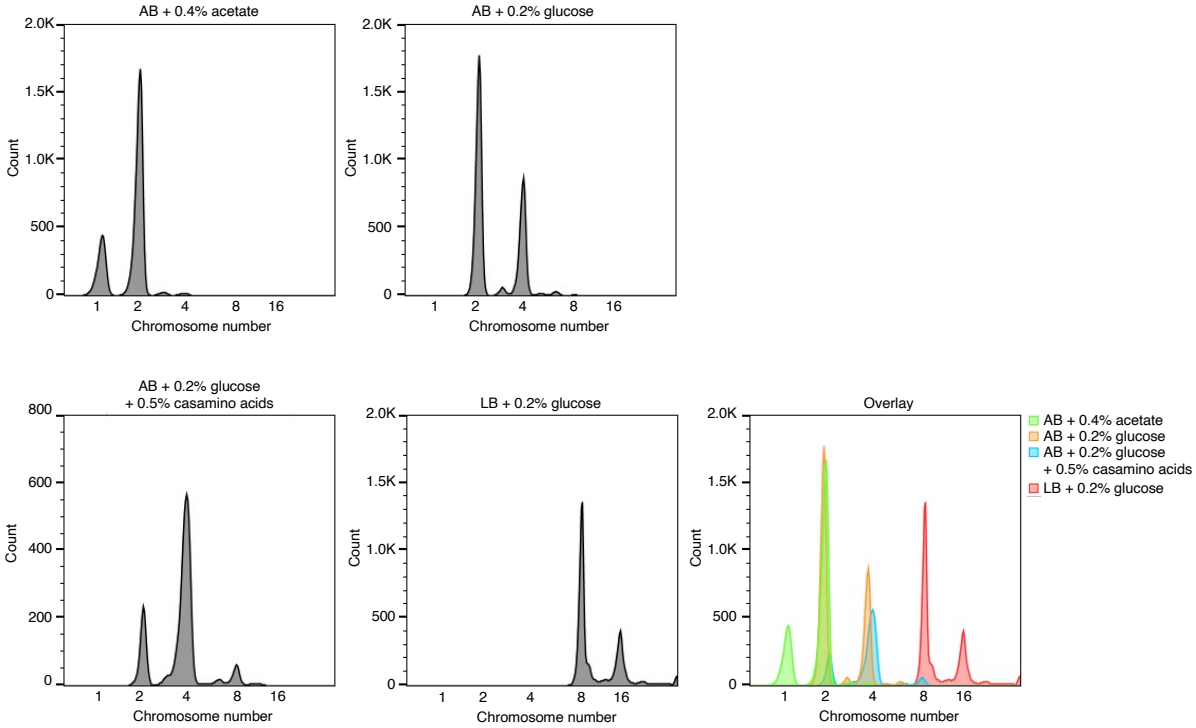

Figure S8 – Replication run-out assay standards

Flow cytometry of *E. coli* MG1655 cells grown in media supporting different growth rates followed by replication run-out assay. Cells were grown in AB minimal medium supplemented with either 0.4% acetate, 0.2% glucose, or 0.2% glucose + 0.5% casamino acids, or LB supplemented 0.2% glucose at 37°C with aeration before being treated with rifampicin, cephalexin and stained with Sytox Green. Fluorescence is plotted and represents chromosomal content for each cell with chromosome numbers for each peak marked. An overlay of the separate data panels is presented.

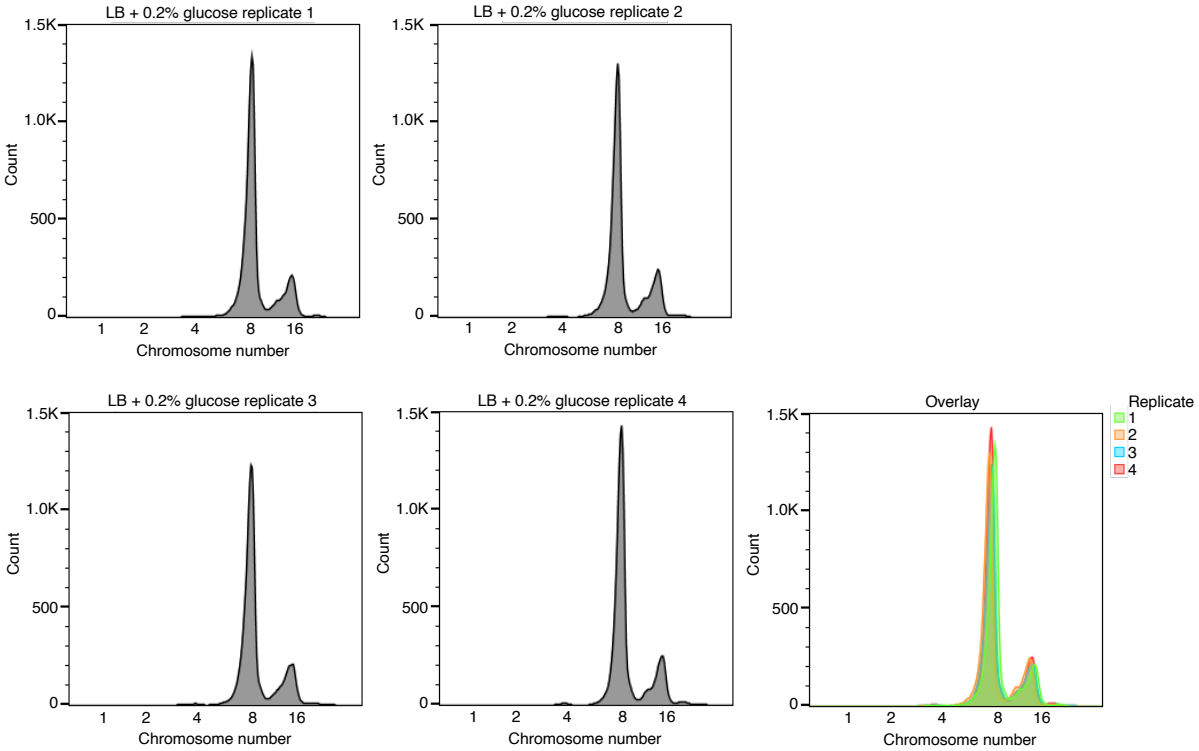

Figure S9 – Reproducibility of replication run-out assays for the parent strain
Flow cytometry of *E. coli* LCE-18 cells grown in LB supplemented with 0.2% glucose at 37°C with aeration before being treated with rifampicin, cephalexin and stained with Sytox Green. Fluorescence is plotted and represents chromosomal content for each cell with chromosome numbers for each peak marked. Each experiment was repeated on 4 separate occasions and an overlay of the separate data panels is presented.

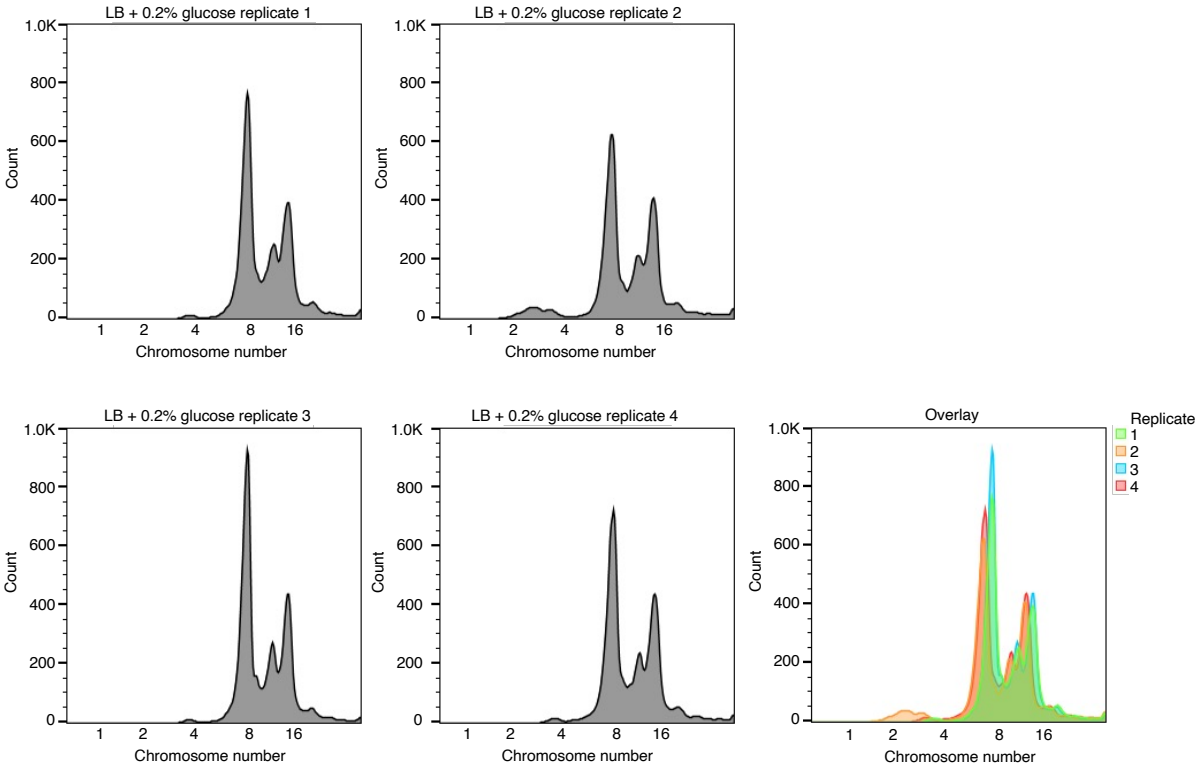

Figure S10 - Reproducibility of replication run-out assays for the Δ*bamB* strain
Flow cytometry of *E. coli* LCE-18 Δ*bamB* cells grown in LB supplemented with 0.2% glucose at 37°C with aeration before being treated with rifampicin, cephalexin and stained with Sytox Green. Fluorescence is plotted and represents chromosomal content for each cell with chromosome numbers for each peak marked. Each experiment was repeated on 4 separate occasions and an overlay of the separate data panels is presented.

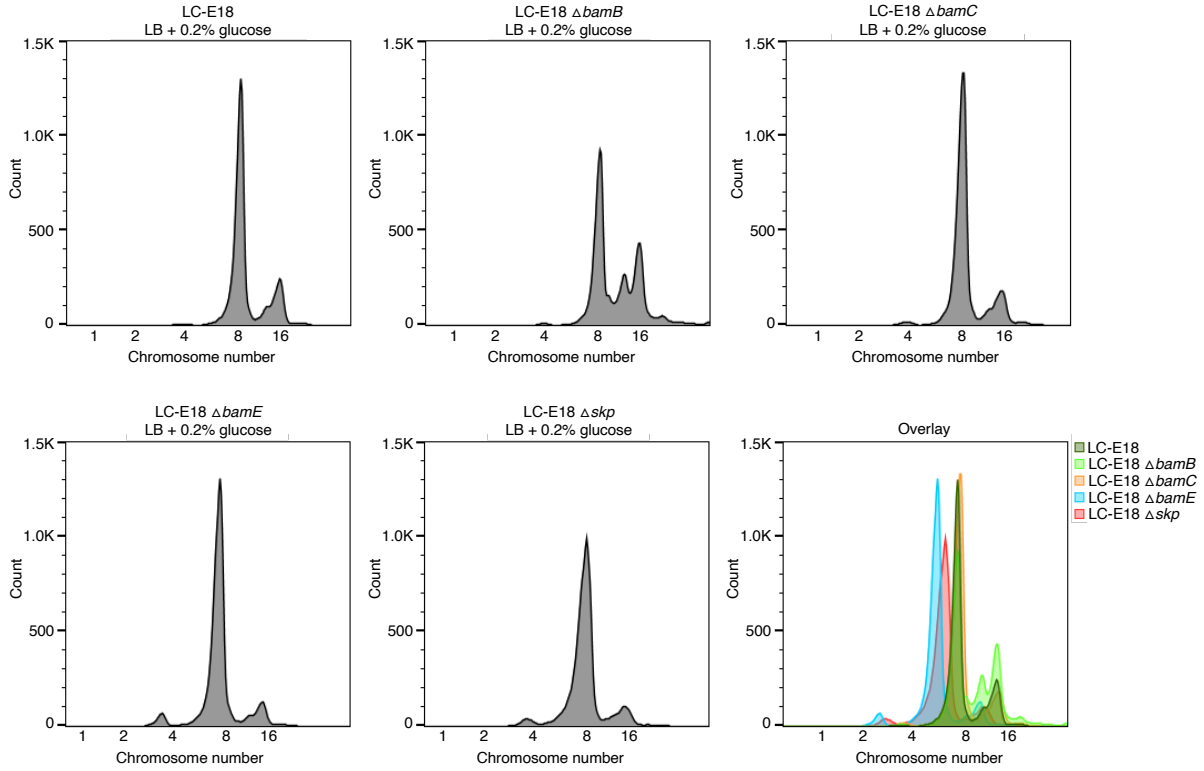

Figure S11 – Replication run-out assays for the parent, Δ*bamB*, Δ*bamC*, Δ*bamE* and Δ*skp* strains

Flow cytometry of *E. coli* LCE-18 WT parent, Δ*bamB*, Δ*bamC*, Δ*bamE* or Δ*skp* cells grown in LB supplemented with 0.2% glucose at 37°C with aeration before being treated with rifampicin, cephalexin and stained with Sytox Green. Fluorescence is plotted and represents chromosomal content for each cell with chromosome numbers for each peak marked. An overlay of the separate data panels is presented.

785 **Materials and methods**

786 **Bacterial strains and culture conditions.**

787 For TraDIS experiments and phenotypic profiling, the parent strain was *E. coli* K-12 BW25113.
788 The *E. coli* Δ*bamB*, Δ*bamC*, Δ*bamE*, Δ*surA*, Δ*skp* and Δ*degP* mutants were generated by
789 transferring the relevant allele from the Keio library [106] into the clean parent strain by P1
790 transduction [107]. The *kan*^{R} cassette was then removed by using the pCP20 plasmid [108] to
791 leave a small in-frame 34 amino acid peptide consisting of residues from the FRT scar and
792 the first amino acid and last seven of the target gene. These strains were then used for
793 construction of transposon libraries and phenotypic profiling. The same approach was used
794 for construction of the *E. coli* Δ*wecA*::*aph*, Δ*wecD*::*aph*, Δ*wecF*::*aph*, Δ*ompT::aph,* Δ*dapF*::*aph*
795 and Δ*diaA::aph* mutants. The *diaA::aph* allele was also transferred into the Δ*bamB* derivative
796 of *E. coli* BW25113 to generate the Δ*bamB*Δ*diaA::aph* double mutant. The *dapF::aph* allele
797 was also transferred from the Keio library into Δ*bamB*, Δ*bamC*, Δ*bamE*, Δ*surA*, Δ*skp* and
798 Δ*degP* mutants in the presence of 1 mM *meso*-diaminopimelate in order to generate double
799 mutants. The Δ*rcsF*Δ*lpp*Δ*pgsA*Δ*surA* mutant was generated by transfer of alleles from the
800 Keio library and subsequent removal of the *kan*^{R} cassette by use of the pCP20 plasmid before
801 incorporation of the next allele by P1 transduction. The *E. coli* Δ*gmhA*::*aph,* Δ*gmhB*::*aph,*
802 Δ*hldE*::*aph,* Δ*waaD*::*aph,* Δ*waaC*::*aph,* Δ*waaF::aph,* Δ*waaP::aph,* Δ*waaG::aph,* Δ*waaY::aph*
803 mutants were created by using λ-Red recombination, as previously described for single-step
804 gene inactivation [109]. All mutants were confirmed by polymerase chain reaction and strains
805 were routinely cultured on LB agar and LB broth. The dCas9 expressing strain *E. coli* LC-E18
806 and the pSGRNA plasmid was a gift from David Bikard (Addgene plasmid # 115924) and has
807 been described previously [110]. The *E. coli* LC-E18 Δ*bamB* derivative was constructed as
808 described for the BW25113 Δ*bamB* derivative with the *kan*^{R} cassette removed in order to allow
809 selection of the pSGRNA plasmid in this background. All strains used in this study are listed
810 in **Table S3**. Bacterial cultures were grown at 37°C unless otherwise stated. Where stated,
811 the medium was supplemented with kanamycin (50 µg/ml), carbenicillin (100 µg/ml), and

812 *meso*-DAP (1 mM). For micro-dilution survival assays, bacteria were grown in 5 ml LB
813 medium at 37°C with aeration for ~16 hours. Cultures were normalised by optical density to
814 OD_{600} = 1.00, 10-fold serially diluted in LB, and 2 µl of each dilution was inoculated onto LB
815 agar plates.
816
817 **Phenotypic screening**
818 The *E. coli* K-12 BW25113 parent strain, Δ*bamB*, Δ*bamC*, Δ*bamE*, Δ*surA*, Δ*skp* and Δ*degP*
819 mutants were screened against diverse stress conditions to phenotypically profile the mutants.
820 Strains were arrayed in 384-well format and inoculated on 2% agar LB plates using a BM3-
821 BC robot (S&P Robotic Inc.). In addition, the mutants and the wild type were subsequently
822 inoculated on LB agar plates containing different stress conditions. The inoculated plates were
823 incubated for 12 to 14 hours at 37°C before being imaged under controlled lighting with an 18-
824 megapixel Canon rebelT3i (Canon) camera on the BM3-BC robot (S&P Robotic Inc.). Images
825 of the plates were analysed using the software IRIS, which measured the size, opacity and
826 circularity of each colony [27]. A total of 4 replica plates were generated for each stress
827 condition. Fitness of the mutants was then scored and analysed using the ChemGAPP Small
828 software [28]. Mean colony size for the mutant in each condition was compared to the mean
829 colony size of that mutant in the LB agar condition, which was normalised to a fitness score of
830 1 [28]. Fitness scores below 1 represent decreased fitness, as a function of colony size
831 compared to growth on LB agar, and scores above 1 indicate increased fitness in that
832 condition. Each of the plates contained 56 replicates for the parent BW25113 strain (WT),
833 Δ*bamB*, Δ*bamC*, Δ*bamE* and Δ*degP* strains with 52 replicates for Δ*surA* and Δ*skp* for plate
834 space requirements. There were 4 replicate plates for each condition, all of which were treated
835 as individual replicates and compared to their respective wild type parent replicates on each
836 plate before the average was taken. The probability that the two means are equal across
837 replicates was obtained by a one-way ANOVA. Correlation of fitness ratios for each strain was
838 assessed by calculating the Pearson correlation coefficient for averaged fitness scores across
839 replicates using Python before being plotted as a heatmap.

840

841 **TraDIS library construction**

842 The *E. coli* K-12 BW25113 parent strain, Δ*bamB*, Δ*bamC*, Δ*bamE*, Δ*surA*, Δ*skp* and Δ*degP*
843 mutants were transformed with the EZ-Tn5™ <KAN-2> Tnp Transposome (Cambio) as
844 previously described [32]. Approximately 1 million mutant colonies were pooled, thoroughly
845 mixed and stored in LB supplemented with 15% glycerol at -80°C. DNA was extracted from at
846 least two samples of each transposon library to generate independent sampling replicates for
847 library generation.

848

849 **Sequencing of TraDIS libraries**

850 Cells from the pooled mutant library were harvested and genomic DNA was extracted for
851 library preparation and sequencing as previously described [32]. Samples were sequenced
852 using an Illumina MiSeq with a 150 cycle v3 cartridge.

853

854 **TraDIS data analysis**

855 Raw data were processed using a series of custom scripts as previously described [32]. The
856 data were trimmed using Fastx barcode splitter and trimmer tools (Pearson *et al.,* 1997) and
857 filtered based on inline indexes. The accuracy of the transposon sequences were checked in
858 two steps: the first 22 bases, allowing for three nucleotide base mismatches and the last 10
859 bases of the transposon, allowing for up to one mismatch. Using Trimmomatic, sequences
860 with less than 20 bases in length were removed (Bolger *et al.,* 2014). TraDIS data were then
861 analysed using BioTraDIS (https://sanger-pathogens.github.io/Bio-Tradis/) [34] and aligned to
862 the *E. coli* BW25113 reference genome CP009273.1, available from NCBI (Tatusova *et al.,*
863 2014). We used SMALT (https://www.sanger.ac.uk/tool/smalt/) as an aligner with zero value
864 for mismatch threshold. We also set the parameter smalt_r, determining how to treat multi-
865 mapping reads, to zero. This avoided repetitive elements to count as essential. We used the
866 scripts *tradis_essentiality.R and tradis_comparison.R* as part of the package to produce the
867 list of essentiality and then to compare the control and test libraries, respectively.

868

869 **Membrane fluidity assay**

870 Membrane fluidity was measured using the membrane fluidity kit (Abcam: ab189819), as
871 previously described, but with minor modifications [104]. Bacterial strains were grown to mid-
872 exponential phase (OD_{600} = ~0.4-0.6) in LB medium. Cells were harvested by centrifugation,
873 washed with phosphate buffered saline (PBS) and incubated with labelling mix (10 μM
874 pyrenedecanoic acid (PDA), 0.08% pluronic F-127, in PBS) in the dark for 20 min at 25°C with
875 rocking. Cells were then washed twice in PBS and re-suspended in PBS prior to measuring
876 fluorescence (excitation = 350 nm, emission = either 400 nm or 470 nm). Membrane fluidity
877 was estimated by measuring the ratio of excimer (470 nm) to monomer (400 nm) fluorescence.
878 The emission spectra were compared to unlabelled cells to confirm membrane incorporation
879 and each experiment contained triplicate technical repeats and was then repeated three times.
880 Membrane fluidity of the mutants of interest were expressed relative to the parent *E. coli* strain.
881 Experiments were performed in technical triplicate and were repeated three times. Two
882 sample t-tests were used to assess statistical significance of differences from the WT strain.

883

884 **OmpT *in vivo* fluorescence assay**

885 The OmpT assay for monitoring Bam activity was performed as described previously with
886 minor modifications [10, 16, 40]. Bacterial strains were grown to mid-exponential phase (OD_{600}
887 = ~0.4-0.6) in LB medium and were normalised to OD_{600} of 0.2 in growth media. The cell
888 suspension (5 μl) was then added to 95 μl of 25 μM fluorogenic peptide, Abz-ARRAY(NO_2)-
889 NH_2, diluted in PBS. Fluorescence emission was immediately measured (excitation = 325 nm,
890 emission = 430 nm) over a period of 5 h, with readings every 20 s. OmpT activity was
891 expressed relative to the parent strain. Experiments were performed in technical triplicate and
892 were repeated three times. Two sample t-tests were used to assess statistical significance of
893 differences from the WT strain.

894

895

896 **Phospholipid extraction and thin layer chromatography**

897 Phospholipids were extracted using an adapted Bligh-Dyer method [111]. Bacterial cultures
898 were grown overnight (~16 hours) at 37°C with shaking and cells were harvested by
899 centrifugation. The bacterial cell pellets were resuspended and normalised to OD_{600} = 3 and
900 mixed with methanol and chloroform (2:1). The cell suspension was incubated at 50°C for 30
901 min before additional chloroform and water was added to the samples to produce a final ratio
902 2:2:1.8 of methanol/chloroform/water. Following centrifugation, the phospholipid-containing
903 phase was extracted and dried under nitrogen before being stored at -20˚C. Samples were re-
904 dissolved in chloroform before being separated by thin layer chromatography on silica gel
905 membrane using a solvent system that consisted of chloroform, methanol, acetic acid
906 (65:25:10). The plate was subsequently stained with phosphomolybdic acid (PMA) and
907 warmed until the lipid species were visible.

908

909 **Efficiency of plating assay**

910 Efficiency of plating assays were completed as previously described [112]. Cells were grown
911 overnight in LB (supplemented with 1 mM *meso*DAP where indicated) before being normalised
912 to OD_{600} = 1.00 and serially diluted 1:10. Following dilution, 2 μl was spotted on agar plates
913 containing supplements where indicated and incubated at 37°C for ~16 hours before being
914 imaged.

915

916 **Genetic interaction analysis**

917 For genetic interaction analysis, overnight cultures were diluted 1/100 and then grown to OD_{600}
918 = 0.8-1. Cultures were then spread on LB agar plates using sterile glass beads to create
919 source plates, before being incubated for 12 to 14 hours at 37˚C. Each strain was arrayed on
920 LB agar plates, from the source plates, to form 384 colonies of 96 replicates for each strain
921 using a BM3-BC robot (S&P Robotic Inc.). Plates were incubated at 37˚C for 12 to 14 hours.
922 The plate was then imaged under controlled lighting, with an 18-megapixel Canon rebelT3i

923 (Canon) camera on the BM3-BC robot (S&P Robotic Inc.). Images were then analysed using
924 the software called IRIS to measure the size, opacity and circularity of each colony on the
925 plates [27]. Fitness of the mutants was then analysed and compared using the software
926 ChemGAPP GI [28].
927
928 **Flow cytometry analysis**
929 Chromosome number measurements were performed as described previously, but with
930 several modifications [71]. Briefly, cells were grown with aeration at 37°C until OD_{600}=0.15 in
931 LB medium supplemented with 0.2% glucose. Samples were collected, treated with 150 µg/ml
932 rifampicin, and 10 µg/ml cephalexin and incubated for 4 h at 37ºC with mixing. Incubation with
933 antibiotics results in cells containing an integral number of chromosomes, corresponding to
934 the number of replication origins at the time of drug treatment. Subsequently, cells were
935 harvested, washed with TBS (20 mM Tris-HCl pH 7.5, 130 mM NaCl) and fixed with cold 70%
936 ethanol overnight. Additional samples were collected at OD_{600}=0.15 without antibiotic
937 treatment and fixed as above.
938 Prior to flow cytometry analysis, cells were resuspended in 50 mM sodium citrate followed by
939 RNA digestion with RNase A for 4 h. Chromosomal DNA was stained with 2 mM Sytox Green
940 (Invitrogen) and DNA content per cell was measured with BD FACS Calibur at 488 nm Argon
941 Ion laser. MG1655 (WT) strain grown in AB medium containing one of the following carbon
942 sources: 0.4% sodium acetate, 0.2% glucose, 0.2% glucose + 0.5% casamino acids or in LB
943 medium with 0.2% glucose, treated with antibiotics, fixed and stained as above was used as
944 a standard for each flow cytometry measurement, indicating cells containing 1/2 , 2/4, 4/8 or
945 8/16 chromosomes, respectively. Flow cytometry data was analyzed using FlowJo ver. 10.8.0.
946
947 **Conservation analysis**
948 Reference genomes were downloaded for each species from NCBI in fasta format and
949 annotated using Prokka [113]. The 16s rRNA sequence for each species was then extracted

950 from Prokka ffn files in fasta format. A Kmer based neighbour joining tree was produced via
951 extracting a one-step sliding window of 8 base kmers from each 16s rRNA sequence.
952 Following this, the number of unique kmers was counted for each species in order to produce
953 a Kmer profile. The Jaccard similarity between each species Kmer profiles was then used to
954 produce a distance matrix. This distance matrix was input into the R module ape::nj to produce
955 the neighbour joining tree. The neighbour joining tree was reformatted as a nexus file and
956 visualised within Figtree (http://tree.bio.ed.ac.uk/software/figtree/), where the tree was rooted
957 at the midpoint and branches were transformed to become proportional.
958 To count the instances of the proteins BamA, BamB, BamC, BamD, BamE, DegP, SurA, and
959 Skp, hmmsearch was used to extract proteins with the relevant domains from the Prokka
960 annotated faa files. The Pfam domains used were PF01103, PF13360, PF06804, PF13525,
961 PF04355, PF09312 and PF03938 for BamA, BamB, BamC, BamD, BamE, SurA, and Skp,
962 respectively. For DegP, both PF00595 and PF13180 were used and the intersect taken. An
963 e-value of 0.001 was used as a threshold for significant hits by hmmsearch. For BamA, hits
964 annotated as the query protein were inputted into hmmscan and hits with at least one POTRA
965 domain and an Omp85 domain were counted as true BamA hits. Hits containing a Tam-
966 POTRA domain were excluded. Where a hit had only an Omp85 gene, the adjacent gene was
967 checked for the POTRA domains. For BamB, any hmmsearch hits annotated as BamB or
968 hypothetical proteins by Prokka were input into SignalP 6.0 [73] and hmmscan. Proteins
969 assigned a LIPO (Sec/SPII) signal peptide within SignalP 6.0, with only one PQQ_2 domain
970 within hmmscan were selected as true BamB hits. For BamC, all hits from hmmsearch were
971 inputted into hmmscan to confirm the presence of the Lipoprotein-18 domain. Hits were also
972 inputted into Phmmer and proteins with significant homology to BamC were counted as true
973 hits. For BamD, hypothetical proteins and BamD hits were inputted into hmmscan and
974 Phmmer and those with homology to BamD and a non-outcompeted YfiO domain counted as
975 true hits. For BamE, hypothetical proteins and BamE hits were inputted into hmmscan and
976 those with a singular SmpA_OmlA domain were counted as true hits. For DegP hypothetical
977 proteins and DegP hits were inputted into hmmscan. If a hit had a PDZ type domain,

978 Peptidase_M50 domain or Trypsin_2 domain then it was visualised on Pfam and manually
979 assigned as DegP based on structure. If a DegP hit had any other type of domain, it was
980 discounted. For SurA, all hits were run through hmmscan and Phmmer. Those with a SurA_N
981 domain, Rotamase domain and a Rotamase_3 domain and homologous to SurA within
982 Phmmer were counted. For Skp, all hits were run through Phmmer and only hits with only an
983 OmpH domain and with homology to Skp counted as true hits. Finally, the neighbour-joining
984 tree was edited in iTOL [76] to produce the heatmap of gene counts.

985 **References**

986

987 1. Konovalova A, Kahne DE, Silhavy TJ. Outer Membrane Biogenesis. Annu Rev Microbiol.
988 2017;71:539-56. Epub 2017/09/10. doi: 10.1146/annurev-micro-090816-093754. PubMed
989 PMID: 28886680; PubMed Central PMCID: PMCPMC5778897.
990 2. Rollauer SE, Sooreshjani MA, Noinaj N, Buchanan SK. Outer membrane protein
991 biogenesis in Gram-negative bacteria. Philos Trans R Soc Lond B Biol Sci. 2015;370(1679). Epub
992 2015/09/16. doi: 10.1098/rstb.2015.0023. PubMed PMID: 26370935; PubMed Central PMCID:
993 PMCPMC4632599.
994 3. Ruiz N, Kahne D, Silhavy TJ. Advances in understanding bacterial outer-membrane
995 biogenesis. Nat Rev Microbiol. 2006;4(1):57-66. Epub 2005/12/17. doi: 10.1038/nrmicro1322.
996 PubMed PMID: 16357861.
997 4. Rizzitello AE, Harper JR, Silhavy TJ. Genetic evidence for parallel pathways of chaperone
998 activity in the periplasm of Escherichia coli. J Bacteriol. 2001;183(23):6794-800. Epub
999 2001/11/08. doi: 10.1128/jb.183.23.6794-6800.2001. PubMed PMID: 11698367; PubMed
1000 Central PMCID: PMCPMC95519.
1001 5. Sklar JG, Wu T, Kahne D, Silhavy TJ. Defining the roles of the periplasmic chaperones
1002 SurA, Skp, and DegP in Escherichia coli. Genes Dev. 2007;21(19):2473-84. Epub 2007/10/03.
1003 doi: 10.1101/gad.1581007. PubMed PMID: 17908933; PubMed Central PMCID:
1004 PMCPMC1993877.
1005 6. Li G, He C, Bu P, Bi H, Pan S, Sun R, et al. Single-Molecule Detection Reveals Different
1006 Roles of Skp and SurA as Chaperones. ACS Chem Biol. 2018;13(4):1082-9. Epub 2018/03/16.
1007 doi: 10.1021/acschembio.8b00097. PubMed PMID: 29543429.
1008 7. Wang X, Peterson JH, Bernstein HD. Bacterial Outer Membrane Proteins Are Targeted
1009 to the Bam Complex by Two Parallel Mechanisms. mBio. 2021;12(3). Epub 20210504. doi:
1010 10.1128/mBio.00597-21. PubMed PMID: 33947759; PubMed Central PMCID:
1011 PMCPMC8262991.
1012 8. Combs AN, Silhavy TJ. The sacrificial adaptor protein Skp functions to remove stalled
1013 substrates from the β-barrel assembly machine. Proc Natl Acad Sci U S A. 2022;119(1). doi:
1014 10.1073/pnas.2114997119. PubMed PMID: 34969846; PubMed Central PMCID:
1015 PMCPMC8740687.
1016 9. Wu T, Malinverni J, Ruiz N, Kim S, Silhavy TJ, Kahne D. Identification of a
1017 multicomponent complex required for outer membrane biogenesis in Escherichia coli. Cell.
1018 2005;121(2):235-45. Epub 2005/04/27. doi: 10.1016/j.cell.2005.02.015. PubMed PMID:
1019 15851030.
1020 10. Hagan CL, Kim S, Kahne D. Reconstitution of outer membrane protein assembly from
1021 purified components. Science. 2010;328(5980):890-2. Epub 2010/04/10. doi:
1022 10.1126/science.1188919. PubMed PMID: 20378773; PubMed Central PMCID: PMC2873164.
1023 11. Sánchez-Pulido L, Devos D, Genevrois S, Vicente M, Valencia A. POTRA: a conserved
1024 domain in the FtsQ family and a class of beta-barrel outer membrane proteins. Trends in
1025 biochemical sciences. 2003;28(10):523-6. Epub 2003/10/16. doi: 10.1016/j.tibs.2003.08.003.
1026 PubMed PMID: 14559180.
1027 12. Gentle IE, Burri L, Lithgow T. Molecular architecture and function of the Omp85 family
1028 of proteins. Mol Microbiol. 2005;58(5):1216-25. Epub 2005/11/30. doi: 10.1111/j.1365-
1029 2958.2005.04906.x. PubMed PMID: 16313611.
1030 13. Knowles TJ, Jeeves M, Bobat S, Dancea F, McClelland D, Palmer T, et al. Fold and
1031 function of polypeptide transport-associated domains responsible for delivering unfolded

1032 proteins to membranes. Mol Microbiol. 2008;68(5):1216-27. Epub 2008/04/24. doi:
1033 10.1111/j.1365-2958.2008.06225.x. PubMed PMID: 18430136.
1034 14. Dong C, Hou HF, Yang X, Shen YQ, Dong YH. Structure of Escherichia coli BamD and its
1035 functional implications in outer membrane protein assembly. Acta Crystallogr D Biol
1036 Crystallogr. 2012;68(Pt 2):95-101. Epub 2012/01/28. doi: 10.1107/s0907444911051031.
1037 PubMed PMID: 22281737.
1038 15. Sandoval CM, Baker SL, Jansen K, Metzner SI, Sousa MC. Crystal structure of BamD: an
1039 essential component of the β-Barrel assembly machinery of gram-negative bacteria. J Mol Biol.
1040 2011;409(3):348-57. Epub 2011/04/06. doi: 10.1016/j.jmb.2011.03.035. PubMed PMID:
1041 21463635; PubMed Central PMCID: PMCPMC3098899.
1042 16. Iadanza MG, Higgins AJ, Schiffrin B, Calabrese AN, Brockwell DJ, Ashcroft AE, et al.
1043 Lateral opening in the intact beta-barrel assembly machinery captured by cryo-EM. Nat
1044 Commun. 2016;7:12865. Epub 2016/10/01. doi: 10.1038/ncomms12865. PubMed PMID:
1045 27686148; PubMed Central PMCID: PMC5056442.
1046 17. Bakelar J, Buchanan SK, Noinaj N. The structure of the beta-barrel assembly machinery
1047 complex. Science. 2016;351(6269):180-6. Epub 2016/01/09. doi: 10.1126/science.aad3460.
1048 PubMed PMID: 26744406; PubMed Central PMCID: PMC4883095.
1049 18. Gu Y, Li H, Dong H, Zeng Y, Zhang Z, Paterson NG, et al. Structural basis of outer
1050 membrane protein insertion by the BAM complex. Nature. 2016;531(7592):64-9. Epub
1051 2016/02/24. doi: 10.1038/nature17199. PubMed PMID: 26901871.
1052 19. Browning DF, Bavro VN, Mason JL, Sevastsyanovich YR, Rossiter AE, Jeeves M, et al.
1053 Cross-species chimeras reveal BamA POTRA and β-barrel domains must be fine-tuned for
1054 efficient OMP insertion. Mol Microbiol. 2015;97(4):646-59. Epub 2015/05/07. doi:
1055 10.1111/mmi.13052. PubMed PMID: 25943387; PubMed Central PMCID: PMCPMC4950039.
1056 20. Knowles TJ, Browning DF, Jeeves M, Maderbocus R, Rajesh S, Sridhar P, et al. Structure
1057 and function of BamE within the outer membrane and the beta-barrel assembly machine.
1058 EMBO Rep. 2011;12(2):123-8. Epub 2011/01/08. doi: 10.1038/embor.2010.202. PubMed
1059 PMID: 21212804; PubMed Central PMCID: PMC3049429.
1060 21. Hart EM, Silhavy TJ. Functions of the BamBCDE Lipoproteins Revealed by Bypass
1061 Mutations in BamA. J Bacteriol. 2020;202(21). Epub 2020/08/21. doi: 10.1128/jb.00401-20.
1062 PubMed PMID: 32817097; PubMed Central PMCID: PMCPMC7549358.
1063 22. Konovalova A, Mitchell AM, Silhavy TJ. A lipoprotein/beta-barrel complex monitors
1064 lipopolysaccharide integrity transducing information across the outer membrane. Elife. 2016;5.
1065 Epub 2016/06/11. doi: 10.7554/eLife.15276. PubMed PMID: 27282389; PubMed Central
1066 PMCID: PMC4942254.
1067 23. Tata M, Konovalova A. Improper Coordination of BamA and BamD Results in Bam
1068 Complex Jamming by a Lipoprotein Substrate. mBio. 2019;10(3). Epub 2019/05/23. doi:
1069 10.1128/mBio.00660-19. PubMed PMID: 31113900; PubMed Central PMCID:
1070 PMCPMC6529637.
1071 24. Kumar S, Konovalova A. BamE directly interacts with BamA and BamD coordinating
1072 their functions. Mol Microbiol. 2023;120(3):397-407. doi:
1073 https://doi.org/10.1111/mmi.15127.
1074 25. Hart EM, Gupta M, Wühr M, Silhavy TJ. The Synthetic Phenotype of ΔbamB ΔbamE
1075 Double Mutants Results from a Lethal Jamming of the Bam Complex by the Lipoprotein RcsF.
1076 mBio. 2019;10(3). Epub 2019/05/23. doi: 10.1128/mBio.00662-19. PubMed PMID: 31113901;
1077 PubMed Central PMCID: PMCPMC6529638.

1078 26. Charlson ES, Werner JN, Misra R. Differential effects of yfgL mutation on Escherichia
1079 coli outer membrane proteins and lipopolysaccharide. J Bacteriol. 2006;188(20):7186-94. Epub
1080 2006/10/04. doi: 10.1128/jb.00571-06. PubMed PMID: 17015657; PubMed Central PMCID:
1081 PMCPMC1636225.
1082 27. Kritikos G, Banzhaf M, Herrera-Dominguez L, Koumoutsi A, Wartel M, Zietek M, et al. A
1083 tool named Iris for versatile high-throughput phenotyping in microorganisms. Nature
1084 microbiology. 2017;2:17014. Epub 2017/02/18. doi: 10.1038/nmicrobiol.2017.14. PubMed
1085 PMID: 28211844; PubMed Central PMCID: PMCPMC5464397.
1086 28. Doherty HM, Kritikos G, Galardini M, Banzhaf M, Moradigaravand D. ChemGAPP: a tool
1087 for chemical genomics analysis and phenotypic profiling. Bioinformatics. 2023;39(4). Epub
1088 2023/04/05. doi: 10.1093/bioinformatics/btad171. PubMed PMID: 37014365; PubMed
1089 Central PMCID: PMCPMC10085634.
1090 29. Spiess C, Beil A, Ehrmann M. A temperature-dependent switch from chaperone to
1091 protease in a widely conserved heat shock protein. Cell. 1999;97(3):339-47. Epub 1999/05/13.
1092 doi: 10.1016/s0092-8674(00)80743-6. PubMed PMID: 10319814.
1093 30. Langridge GC, Phan MD, Turner DJ, Perkins TT, Parts L, Haase J, et al. Simultaneous
1094 assay of every Salmonella Typhi gene using one million transposon mutants. Genome Res.
1095 2009;19(12):2308-16. Epub 2009/10/15. doi: 10.1101/gr.097097.109. PubMed PMID:
1096 19826075; PubMed Central PMCID: PMCPMC2792183.
1097 31. Cain AK, Barquist L, Goodman AL, Paulsen IT, Parkhill J, van Opijnen T. A decade of
1098 advances in transposon-insertion sequencing. Nat Rev Genet. 2020;21(9):526-40. Epub
1099 2020/06/14. doi: 10.1038/s41576-020-0244-x. PubMed PMID: 32533119; PubMed Central
1100 PMCID: PMCPMC7291929.
1101 32. Goodall ECA, Isom GL, Rooke JL, Pullela K, Icke C, Yang Z, et al. Loss of YhcB results in
1102 dysregulation of coordinated peptidoglycan, LPS and phospholipid synthesis during Escherichia
1103 coli cell growth. PLoS Genet. 2021;17(12):e1009586. Epub 2021/12/24. doi:
1104 10.1371/journal.pgen.1009586. PubMed PMID: 34941903; PubMed Central PMCID:
1105 PMCPMC8741058.
1106 33. Winkle M, Hernández-Rocamora VM, Pullela K, Goodall ECA, Martorana AM, Gray J, et
1107 al. DpaA Detaches Braun's Lipoprotein from Peptidoglycan. mBio. 2021;12(3). Epub
1108 2021/05/06. doi: 10.1128/mBio.00836-21. PubMed PMID: 33947763; PubMed Central PMCID:
1109 PMCPMC8263019.
1110 34. Barquist L, Mayho M, Cummins C, Cain AK, Boinett CJ, Page AJ, et al. The TraDIS toolkit:
1111 sequencing and analysis for dense transposon mutant libraries. Bioinformatics.
1112 2016;32(7):1109-11. Epub 2016/01/23. doi: 10.1093/bioinformatics/btw022. PubMed PMID:
1113 26794317; PubMed Central PMCID: PMCPMC4896371.
1114 35. Cooper S, Helmstetter CE. Chromosome replication and the division cycle of Escherichia
1115 coli B/r. J Mol Biol. 1968;31(4866337):519-40.
1116 36. Sklar JG, Wu T, Gronenberg LS, Malinverni JC, Kahne D, Silhavy TJ. Lipoprotein SmpA is
1117 a component of the YaeT complex that assembles outer membrane proteins in Escherichia coli.
1118 Proc Natl Acad Sci U S A. 2007;104(15):6400-5. Epub 2007/04/04. doi:
1119 10.1073/pnas.0701579104. PubMed PMID: 17404237; PubMed Central PMCID: PMC1851043.
1120 37. Kneidinger B, Marolda C, Graninger M, Zamyatina A, McArthur F, Kosma P, et al.
1121 Biosynthesis pathway of ADP-l-glycero-β-d-manno-heptose in Escherichia coli. J Bacteriol.
1122 2002;184(2):363-9.
1123 38. Gronow S, Brabetz W, Brade H. Comparative functional characterization in vitro of
1124 heptosyltransferase I (WaaC) and II (WaaF) from Escherichia coli. Eur J Biochem.

1125 2000;267(22):6602-11. Epub 2000/10/29. doi: 10.1046/j.1432-1327.2000.01754.x. PubMed
1126 PMID: 11054112.
1127 39. Kadrmas JL, Raetz CR. Enzymatic synthesis of lipopolysaccharide in Escherichia coli.
1128 Purification and properties of heptosyltransferase i. J Biol Chem. 1998;273(5):2799-807. Epub
1129 1998/02/28. doi: 10.1074/jbc.273.5.2799. PubMed PMID: 9446588.
1130 40. Storek KM, Vij R, Sun D, Smith PA, Koerber JT, Rutherford ST. The Escherichia coli β-
1131 Barrel Assembly Machinery Is Sensitized to Perturbations under High Membrane Fluidity. J
1132 Bacteriol. 2019;201(1). Epub 2018/10/17. doi: 10.1128/jb.00517-18. PubMed PMID:
1133 30322857; PubMed Central PMCID: PMCPMC6287456.
1134 41. Yethon JA, Heinrichs DE, Monteiro MA, Perry MB, Whitfield C. Involvement of waaY,
1135 waaQ, and waaP in the modification of Escherichia coli lipopolysaccharide and their role in the
1136 formation of a stable outer membrane. J Biol Chem. 1998;273(41):26310-6. Epub 1998/10/03.
1137 doi: 10.1074/jbc.273.41.26310. PubMed PMID: 9756860.
1138 42. Parker CT, Kloser AW, Schnaitman CA, Stein MA, Gottesman S, Gibson BW. Role of the
1139 rfaG and rfaP genes in determining the lipopolysaccharide core structure and cell surface
1140 properties of Escherichia coli K-12. J Bacteriol. 1992;174(8):2525-38. Epub 1992/04/01. doi:
1141 10.1128/jb.174.8.2525-2538.1992. PubMed PMID: 1348243; PubMed Central PMCID:
1142 PMCPMC205891.
1143 43. Kumar GS, Jagannadham MV, Ray MK. Low-temperature-induced changes in
1144 composition and fluidity of lipopolysaccharides in the antarctic psychrotrophic bacterium
1145 Pseudomonas syringae. J Bacteriol. 2002;184(23):6746-9. Epub 2002/11/12. doi:
1146 10.1128/jb.184.23.6746-6749.2002. PubMed PMID: 12426366; PubMed Central PMCID:
1147 PMCPMC135421.
1148 44. Storek KM, Auerbach MR, Shi H, Garcia NK, Sun D, Nickerson NN, et al. Monoclonal
1149 antibody targeting the β-barrel assembly machine of Escherichia coli is bactericidal. Proc Natl
1150 Acad Sci U S A. 2018;115(14):3692-7. Epub 2018/03/21. doi: 10.1073/pnas.1800043115.
1151 PubMed PMID: 29555747; PubMed Central PMCID: PMCPMC5889671.
1152 45. Kuhn HM, Meier-Dieter U, Mayer H. ECA, the enterobacterial common antigen. FEMS
1153 Microbiol Rev. 1988;4(3):195-222. Epub 1988/09/01. doi: 10.1111/j.1574-
1154 6968.1988.tb02743.x. PubMed PMID: 3078744.
1155 46. Kunin CM. SEPARATION, CHARACTERIZATION, AND BIOLOGICAL SIGNIFICANCE OF A
1156 COMMON ANTIGEN IN ENTEROBACTERIACEAE. J Exp Med. 1963;118(4):565-86. Epub
1157 1963/10/01. doi: 10.1084/jem.118.4.565. PubMed PMID: 14067906; PubMed Central PMCID:
1158 PMCPMC2137670.
1159 47. Sivaraman J, Sauvé V, Matte A, Cygler M. Crystal structure of Escherichia coli glucose-
1160 1-phosphate thymidylyltransferase (RffH) complexed with dTTP and Mg2+. J Biol Chem.
1161 2002;277(46):44214-9. Epub 2002/08/13. doi: 10.1074/jbc.M206932200. PubMed PMID:
1162 12171937.
1163 48. Marolda CL, Valvano MA. Genetic analysis of the dTDP-rhamnose biosynthesis region
1164 of the Escherichia coli VW187 (O7:K1) rfb gene cluster: identification of functional homologs
1165 of rfbB and rfbA in the rff cluster and correct location of the rffE gene. J Bacteriol.
1166 1995;177(19):5539-46. Epub 1995/10/01. doi: 10.1128/jb.177.19.5539-5546.1995. PubMed
1167 PMID: 7559340; PubMed Central PMCID: PMCPMC177362.
1168 49. Rai AK, Mitchell AM. Enterobacterial Common Antigen: Synthesis and Function of an
1169 Enigmatic Molecule. mBio. 2020;11(4). Epub 2020/08/14. doi: 10.1128/mBio.01914-20.
1170 PubMed PMID: 32788387; PubMed Central PMCID: PMCPMC7439462.

1171 50. Rai AK, Carr JF, Bautista DE, Wang W, Mitchell AM. ElyC and Cyclic Enterobacterial
1172 Common Antigen Regulate Synthesis of Phosphoglyceride-Linked Enterobacterial Common
1173 Antigen. mBio. 2021;12(6):e0284621. Epub 2021/11/24. doi: 10.1128/mBio.02846-21.
1174 PubMed PMID: 34809459; PubMed Central PMCID: PMCPMC8609368.
1175 51. Schmidt G, Mannel D, Mayer H, Whang HY, Neter E. Role of a lipopolysaccharide gene
1176 for immunogenicity of the enterobacterial common antigen. J Bacteriol. 1976;126(2):579-86.
1177 Epub 1976/05/01. doi: 10.1128/jb.126.2.579-586.1976. PubMed PMID: 57114; PubMed
1178 Central PMCID: PMCPMC233189.
1179 52. Kuhn HM, Neter E, Mayer H. Modification of the lipid moiety of the enterobacterial
1180 common antigen by the "Pseudomonas factor". Infection and immunity. 1983;40(2):696-700.
1181 Epub 1983/05/01. doi: 10.1128/iai.40.2.696-700.1983. PubMed PMID: 6404831; PubMed
1182 Central PMCID: PMCPMC264911.
1183 53. Morris KN, Mitchell AM. Phosphatidylglycerol Is the Lipid Donor for Synthesis of
1184 Phospholipid-Linked Enterobacterial Common Antigen. J Bacteriol. 2023:e0040322. Epub
1185 2023/01/10. doi: 10.1128/jb.00403-22. PubMed PMID: 36622229.
1186 54. Rowlett VW, Mallampalli V, Karlstaedt A, Dowhan W, Taegtmeyer H, Margolin W, et al.
1187 Impact of Membrane Phospholipid Alterations in Escherichia coli on Cellular Function and
1188 Bacterial Stress Adaptation. J Bacteriol. 2017;199(13). Epub 2017/04/26. doi:
1189 10.1128/jb.00849-16. PubMed PMID: 28439040; PubMed Central PMCID: PMCPMC5472821.
1190 55. Kikuchi S, Shibuya I, Matsumoto K. Viability of an Escherichia coli pgsA null mutant
1191 lacking detectable phosphatidylglycerol and cardiolipin. J Bacteriol. 2000;182(2):371-6. Epub
1192 2000/01/12. doi: 10.1128/jb.182.2.371-376.2000. PubMed PMID: 10629182; PubMed Central
1193 PMCID: PMCPMC94285.
1194 56. Suzuki M, Hara H, Matsumoto K. Envelope disorder of Escherichia coli cells lacking
1195 phosphatidylglycerol. J Bacteriol. 2002;184(19):5418-25. Epub 2002/09/10. doi:
1196 10.1128/jb.184.19.5418-5425.2002. PubMed PMID: 12218030; PubMed Central PMCID:
1197 PMCPMC135371.
1198 57. Mitchell AM, Srikumar T, Silhavy TJ. Cyclic Enterobacterial Common Antigen Maintains
1199 the Outer Membrane Permeability Barrier of Escherichia coli in a Manner Controlled by YhdP.
1200 mBio. 2018;9(4). Epub 2018/08/09. doi: 10.1128/mBio.01321-18. PubMed PMID: 30087168;
1201 PubMed Central PMCID: PMCPMC6083912.
1202 58. Kajimura J, Rahman A, Rick PD. Assembly of cyclic enterobacterial common antigen in
1203 Escherichia coli K-12. J Bacteriol. 2005;187(20):6917-27. Epub 2005/10/04. doi:
1204 10.1128/jb.187.20.6917-6927.2005. PubMed PMID: 16199561; PubMed Central PMCID:
1205 PMCPMC1251615.
1206 59. Richaud C, Higgins W, Mengin-Lecreulx D, Stragier P. Molecular cloning,
1207 characterization, and chromosomal localization of dapF, the Escherichia coli gene for
1208 diaminopimelate epimerase. J Bacteriol. 1987;169(4):1454-9. Epub 1987/04/01. doi:
1209 10.1128/jb.169.4.1454-1459.1987. PubMed PMID: 3031013; PubMed Central PMCID:
1210 PMCPMC211967.
1211 60. Dewey DL, Work E. Diaminopimelic acid decarboxylase. Nature. 1952;169(4300):533-
1212 4. Epub 1952/03/29. doi: 10.1038/169533a0. PubMed PMID: 14929227.
1213 61. Mickiewicz KM, Kawai Y, Drage L, Gomes MC, Davison F, Pickard R, et al. Possible role
1214 of L-form switching in recurrent urinary tract infection. Nat Commun. 2019;10(1):4379. Epub
1215 2019/09/29. doi: 10.1038/s41467-019-12359-3. PubMed PMID: 31558767; PubMed Central
1216 PMCID: PMCPMC6763468.

62. Mengin-Lecreulx D, Michaud C, Richaud C, Blanot D, van Heijenoort J. Incorporation of LL-diaminopimelic acid into peptidoglycan of Escherichia coli mutants lacking diaminopimelate epimerase encoded by dapF. J Bacteriol. 1988;170(5):2031-9. Epub 1988/05/01. doi: 10.1128/jb.170.5.2031-2039.1988. PubMed PMID: 3283102; PubMed Central PMCID: PMCPMC211082.
63. Jameson KH, Wilkinson AJ. Control of initiation of DNA replication in Bacillus subtilis and Escherichia coli. Genes. 2017;8(1):22.
64. Lu M, Campbell JL, Boye E, Kleckner N. SeqA: a negative modulator of replication initiation in E. coli. Cell. 1994;77(3):413-26. Epub 1994/05/06. doi: 10.1016/0092-8674(94)90156-2. PubMed PMID: 8011018.
65. Torheim NK, Skarstad K. Escherichia coli SeqA protein affects DNA topology and inhibits open complex formation at oriC. Embo j. 1999;18(17):4882-8. Epub 1999/09/02. doi: 10.1093/emboj/18.17.4882. PubMed PMID: 10469666; PubMed Central PMCID: PMCPMC1171560.
66. von Freiesleben U, Rasmussen KV, Schaechter M. SeqA limits DnaA activity in replication from oriC in Escherichia coli. Mol Microbiol. 1994;14(7891562):763-72.
67. Kato J, Katayama T. Hda, a novel DnaA-related protein, regulates the replication cycle in Escherichia coli. Embo j. 2001;20(15):4253-62. Epub 2001/08/03. doi: 10.1093/emboj/20.15.4253. PubMed PMID: 11483528; PubMed Central PMCID: PMCPMC149159.
68. Katayama T, Kubota T, Kurokawa K, Crooke E, Sekimizu K. The initiator function of DnaA protein is negatively regulated by the sliding clamp of the E. coli chromosomal replicase. Cell. 1998;94(1):61-71. Epub 1998/07/23. doi: 10.1016/s0092-8674(00)81222-2. PubMed PMID: 9674428.
69. Ishida T, Akimitsu N, Kashioka T, Hatano M, Kubota T, Ogata Y, et al. DiaA, a novel DnaA-binding protein, ensures the timely initiation of Escherichia coli chromosome replication. Journal of Biological Chemistry. 2004;279(44):45546-55.
70. Keyamura K, Fujikawa N, Ishida T, Ozaki S, Su'etsugu M, Fujimitsu K, et al. The interaction of DiaA and DnaA regulates the replication cycle in E. coli by directly promoting ATP–DnaA-specific initiation complexes. Genes & development. 2007;21(16):2083-99.
71. Hawkins M, Atkinson J, McGlynn P. Escherichia coli Chromosome Copy Number Measurement Using Flow Cytometry Analysis. Methods Mol Biol. 2016;1431:151-9. Epub 2016/06/11. doi: 10.1007/978-1-4939-3631-1_12. PubMed PMID: 27283308.
72. Webb CT, Heinz E, Lithgow T. Evolution of the β-barrel assembly machinery. Trends in microbiology. 2012;20(12):612-20. Epub 2012/09/11. doi: 10.1016/j.tim.2012.08.006. PubMed PMID: 22959613.
73. Teufel F, Almagro Armenteros JJ, Johansen AR, Gíslason MH, Pihl SI, Tsirigos KD, et al. SignalP 6.0 predicts all five types of signal peptides using protein language models. Nat Biotechnol. 2022;40(7):1023-5. Epub 2022/01/05. doi: 10.1038/s41587-021-01156-3. PubMed PMID: 34980915; PubMed Central PMCID: PMCPMC9287161 for a fee to commercial users). The revenue from these commercial sales is divided between the program developers and the Technical University of Denmark.
74. Malinverni JC, Silhavy TJ. Assembly of Outer Membrane β-Barrel Proteins: the Bam Complex. EcoSal Plus. 2011;4(2). Epub 2011/12/01. doi: 10.1128/ecosalplus.4.3.8. PubMed PMID: 26442509; PubMed Central PMCID: PMCPMC4231818.
75. Webb CT, Chandrapala D, Oslan SN, Bamert RS, Grinter RD, Dunstan RA, et al. Reductive evolution in outer membrane protein biogenesis has not compromised cell surface complexity

1264 in Helicobacter pylori. Microbiologyopen. 2017;6(6). Epub 2017/10/23. doi:
1265 10.1002/mbo3.513. PubMed PMID: 29055967; PubMed Central PMCID: PMCPMC5727368.
1266 76. Letunic I, Bork P. Interactive Tree Of Life (iTOL) v5: an online tool for phylogenetic tree
1267 display and annotation. Nucleic Acids Res. 2021;49(W1):W293-w6. Epub 2021/04/23. doi:
1268 10.1093/nar/gkab301. PubMed PMID: 33885785; PubMed Central PMCID: PMCPMC8265157.
1269 77. Steenhuis M, van Ulsen P, Martin NI, Luirink J. A ban on BAM: an update on inhibitors
1270 of the β-barrel assembly machinery. FEMS Microbiol Lett. 2021;368(11). Epub 2021/05/29. doi:
1271 10.1093/femsle/fnab059. PubMed PMID: 34048543.
1272 78. Theuretzbacher U, Blasco B, Duffey M, Piddock LJV. Unrealized targets in the discovery
1273 of antibiotics for Gram-negative bacterial infections. Nat Rev Drug Discov. 2023;22(12):957-75.
1274 Epub 20231013. doi: 10.1038/s41573-023-00791-6. PubMed PMID: 37833553.
1275 79. Tomasek D, Rawson S, Lee J, Wzorek JS, Harrison SC, Li Z, et al. Structure of a nascent
1276 membrane protein as it folds on the BAM complex. Nature. 2020;583(7816):473-8. Epub
1277 2020/06/13. doi: 10.1038/s41586-020-2370-1. PubMed PMID: 32528179; PubMed Central
1278 PMCID: PMCPMC7367713.
1279 80. Doyle MT, Jimah JR, Dowdy T, Ohlemacher SI, Larion M, Hinshaw JE, et al. Cryo-EM
1280 structures reveal multiple stages of bacterial outer membrane protein folding. Cell.
1281 2022;185(7):1143-56.e13. Epub 2022/03/17. doi: 10.1016/j.cell.2022.02.016. PubMed PMID:
1282 35294859; PubMed Central PMCID: PMCPMC8985213.
1283 81. Valvano MA. Remodelling of the Gram-negative bacterial Kdo(2)-lipid A and its
1284 functional implications. Microbiology (Reading). 2022;168(4). Epub 2022/04/09. doi:
1285 10.1099/mic.0.001159. PubMed PMID: 35394417.
1286 82. Simpson BW, Trent MS. Pushing the envelope: LPS modifications and their
1287 consequences. Nat Rev Microbiol. 2019;17(7):403-16. Epub 2019/05/31. doi: 10.1038/s41579-
1288 019-0201-x. PubMed PMID: 31142822; PubMed Central PMCID: PMCPMC6913091.
1289 83. Krojer T, Sawa J, Schäfer E, Saibil HR, Ehrmann M, Clausen T. Structural basis for the
1290 regulated protease and chaperone function of DegP. Nature. 2008;453(7197):885-90. Epub
1291 2008/05/23. doi: 10.1038/nature07004. PubMed PMID: 18496527.
1292 84. Rouvière PE, Gross CA. SurA, a periplasmic protein with peptidyl-prolyl isomerase
1293 activity, participates in the assembly of outer membrane porins. Genes Dev. 1996;10(24):3170-
1294 82. Epub 1996/12/15. doi: 10.1101/gad.10.24.3170. PubMed PMID: 8985185.
1295 85. Lazar SW, Kolter R. SurA assists the folding of Escherichia coli outer membrane proteins.
1296 J Bacteriol. 1996;178(6):1770-3. Epub 1996/03/01. doi: 10.1128/jb.178.6.1770-1773.1996.
1297 PubMed PMID: 8626309; PubMed Central PMCID: PMCPMC177866.
1298 86. Jorgenson MA, Kannan S, Laubacher ME, Young KD. Dead-end intermediates in the
1299 enterobacterial common antigen pathway induce morphological defects in Escherichia coli by
1300 competing for undecaprenyl phosphate. Mol Microbiol. 2016;100(1):1-14. Epub 2015/11/26.
1301 doi: 10.1111/mmi.13284. PubMed PMID: 26593043; PubMed Central PMCID:
1302 PMCPMC4845916.
1303 87. Rojas ER, Billings G, Odermatt PD, Auer GK, Zhu L, Miguel A, et al. The outer membrane
1304 is an essential load-bearing element in Gram-negative bacteria. Nature. 2018;559(7715):617-
1305 21. Epub 2018/07/20. doi: 10.1038/s41586-018-0344-3. PubMed PMID: 30022160; PubMed
1306 Central PMCID: PMCPMC6089221.
1307 88. Nichols RJ, Sen S, Choo YJ, Beltrao P, Zietek M, Chaba R, et al. Phenotypic landscape of
1308 a bacterial cell. Cell. 2011;144(1):143-56. Epub 2010/12/28. doi: 10.1016/j.cell.2010.11.052.
1309 PubMed PMID: 21185072; PubMed Central PMCID: PMCPMC3060659.

1310 89. Thewasano N, Germany EM, Maruno Y, Nakajima Y, Shiota T. Categorization of
1311 Escherichia coli Outer Membrane Proteins by Dependence on Accessory Proteins
1312 of the β-barrel Assembly Machinery Complex. Journal of Biological Chemistry. doi:
1313 10.1016/j.jbc.2023.104821.
1314 90. Mamou G, Corona F, Cohen-Khait R, Housden NG, Yeung V, Sun D, et al. Peptidoglycan
1315 maturation controls outer membrane protein assembly. Nature. 2022;606(7916):953-9. Epub
1316 2022/06/16. doi: 10.1038/s41586-022-04834-7. PubMed PMID: 35705811; PubMed Central
1317 PMCID: PMCPMC9242858 competing interests. D.S. is an employee of Genentech, a member
1318 of the Roche Group, and a shareholder in Roche.
1319 91. Wallden M, Fange D, Lundius EG, Baltekin Ö, Elf J. The Synchronization of Replication
1320 and Division Cycles in Individual E. coli Cells. Cell. 2016;166(3):729-39. Epub 2016/07/30. doi:
1321 10.1016/j.cell.2016.06.052. PubMed PMID: 27471967.
1322 92. Si F, Li D, Cox SE, Sauls JT, Azizi O, Sou C, et al. Invariance of Initiation Mass and
1323 Predictability of Cell Size in Escherichia coli. Curr Biol. 2017;27(9):1278-87. Epub 2017/04/19.
1324 doi: 10.1016/j.cub.2017.03.022. PubMed PMID: 28416114; PubMed Central PMCID:
1325 PMCPMC5474944.
1326 93. Harris LK, Theriot JA. Relative Rates of Surface and Volume Synthesis Set Bacterial Cell
1327 Size. Cell. 2016;165(6):1479-92. Epub 2016/06/04. doi: 10.1016/j.cell.2016.05.045. PubMed
1328 PMID: 27259152; PubMed Central PMCID: PMCPMC4933963.
1329 94. Davies BW, Kohanski MA, Simmons LA, Winkler JA, Collins JJ, Walker GC. Hydroxyurea
1330 induces hydroxyl radical-mediated cell death in Escherichia coli. Mol Cell. 2009;36(5):845-60.
1331 Epub 2009/12/17. doi: 10.1016/j.molcel.2009.11.024. PubMed PMID: 20005847; PubMed
1332 Central PMCID: PMCPMC2821657.
1333 95. Nakayashiki T, Mori H. Genome-wide screening with hydroxyurea reveals a link
1334 between nonessential ribosomal proteins and reactive oxygen species production. J Bacteriol.
1335 2013;195(6):1226-35. Epub 2013/01/08. doi: 10.1128/jb.02145-12. PubMed PMID: 23292777;
1336 PubMed Central PMCID: PMCPMC3592001.
1337 96. Sutera VA, Jr., Lovett ST. The role of replication initiation control in promoting survival
1338 of replication fork damage. Mol Microbiol. 2006;60(1):229-39. Epub 2006/03/25. doi:
1339 10.1111/j.1365-2958.2006.05093.x. PubMed PMID: 16556234.
1340 97. Camara JE, Breier AM, Brendler T, Austin S, Cozzarelli NR, Crooke E. Hda inactivation of
1341 DnaA is the predominant mechanism preventing hyperinitiation of Escherichia coli DNA
1342 replication. EMBO Rep. 2005;6(8):736-41. Epub 2005/07/26. doi: 10.1038/sj.embor.7400467.
1343 PubMed PMID: 16041320; PubMed Central PMCID: PMCPMC1369143.
1344 98. Camara JE, Skarstad K, Crooke E. Controlled initiation of chromosomal replication in
1345 Escherichia coli requires functional Hda protein. J Bacteriol. 2003;185(10):3244-8. Epub
1346 2003/05/06. doi: 10.1128/jb.185.10.3244-3248.2003. PubMed PMID: 12730188; PubMed
1347 Central PMCID: PMCPMC154069.
1348 99. Cooper DL, Harada T, Tamazi S, Ferrazzoli AE, Lovett ST. The Role of Replication Clamp-
1349 Loader Protein HolC of Escherichia coli in Overcoming Replication/Transcription Conflicts.
1350 mBio. 2021;12(2). Epub 2021/03/11. doi: 10.1128/mBio.00184-21. PubMed PMID: 33688004;
1351 PubMed Central PMCID: PMCPMC8092217.
1352 100. Sekimizu K, Kornberg A. Cardiolipin activation of dnaA protein, the initiation protein of
1353 replication in Escherichia coli. J Biol Chem. 1988;263(15):7131-5. Epub 1988/05/25. PubMed
1354 PMID: 2835364.
1355 101. Garner J, Durrer P, Kitchen J, Brunner J, Crooke E. Membrane-mediated release of
1356 nucleotide from an initiator of chromosomal replication, Escherichia coli DnaA, occurs with

insertion of a distinct region of the protein into the lipid bilayer. J Biol Chem. 1998;273(9):5167-73. Epub 1998/03/28. doi: 10.1074/jbc.273.9.5167. PubMed PMID: 9478970.

102. d'Alençon E, Taghbalout A, Kern R, Kohiyama M. Replication cycle dependent association of SeqA to the outer membrane fraction of E. coli. Biochimie. 1999;81(8-9):841-6. Epub 1999/11/26. doi: 10.1016/s0300-9084(99)00212-6. PubMed PMID: 10572297.

103. Rotman E, Bratcher P, Kuzminov A. Reduced lipopolysaccharide phosphorylation in Escherichia coli lowers the elevated ori/ter ratio in seqA mutants. Mol Microbiol. 2009;72(5):1273-92. Epub 2009/05/13. doi: 10.1111/j.1365-2958.2009.06725.x. PubMed PMID: 19432803; PubMed Central PMCID: PMCPMC2691451.

104. Bryant JA, Morris FC, Knowles TJ, Maderbocus R, Heinz E, Boelter G, et al. Structure of dual BON-domain protein DolP identifies phospholipid binding as a new mechanism for protein localisation. Elife. 2020;9. Epub 2020/12/15. doi: 10.7554/eLife.62614. PubMed PMID: 33315009; PubMed Central PMCID: PMCPMC7806268.

105. Ranava D, Yang Y, Orenday-Tapia L, Rousset F, Turlan C, Morales V, et al. Lipoprotein DolP supports proper folding of BamA in the bacterial outer membrane promoting fitness upon envelope stress. Elife. 2021;10. Epub 2021/04/14. doi: 10.7554/eLife.67817. PubMed PMID: 33847565; PubMed Central PMCID: PMCPMC8081527.

106. Baba T, Ara T, Hasegawa M, Takai Y, Okumura Y, Baba M, et al. Construction of Escherichia coli K-12 in-frame, single-gene knockout mutants: the Keio collection. Mol Syst Biol. 2006;2:2006.0008. Epub 2006/06/02. doi: 10.1038/msb4100050. PubMed PMID: 16738554; PubMed Central PMCID: PMCPMC1681482.

107. Thomason LC, Costantino N, Court DL. E. coli genome manipulation by P1 transduction. Curr Protoc Mol Biol. 2007;Chapter 1:1.17.1-1..8. Epub 2008/02/12. doi: 10.1002/0471142727.mb0117s79. PubMed PMID: 18265391.

108. Cherepanov PP, Wackernagel W. Gene disruption in Escherichia coli: TcR and KmR cassettes with the option of Flp-catalyzed excision of the antibiotic-resistance determinant. Gene. 1995;158(7789817):9-14.

109. Datsenko KA, Wanner BL. One-step inactivation of chromosomal genes in Escherichia coli K-12 using PCR products. Proc Natl Acad Sci U S A. 2000;97(12):6640-5. Epub 2000/06/01. doi: 10.1073/pnas.120163297. PubMed PMID: 10829079; PubMed Central PMCID: PMC18686.

110. Cui L, Vigouroux A, Rousset F, Varet H, Khanna V, Bikard D. A CRISPRi screen in E. coli reveals sequence-specific toxicity of dCas9. Nat Commun. 2018;9(1):1912. Epub 2018/05/17. doi: 10.1038/s41467-018-04209-5. PubMed PMID: 29765036; PubMed Central PMCID: PMCPMC5954155.

111. Bligh EG, Dyer WJ. A rapid method of total lipid extraction and purification. Can J Biochem Physiol. 1959;37(8):911-7. Epub 1959/08/01. doi: 10.1139/o59-099. PubMed PMID: 13671378.

112. Boelter G, Bryant JA, Doherty H, Wotherspoon P, Alodaini D, Ma X, et al. The lipoprotein DolP affects cell separation in Escherichia coli, but not as an upstream regulator of NlpD. Microbiology (Reading). 2022;168(5). Epub 2022/05/24. doi: 10.1099/mic.0.001197. PubMed PMID: 35604759.

113. Seemann T. Prokka: rapid prokaryotic genome annotation. Bioinformatics. 2014;30(14):2068-9. Epub 2014/03/20. doi: 10.1093/bioinformatics/btu153. PubMed PMID: 24642063.